SG010-MEA-037

WIRE-WRAP ASSEMBLY ENGINEERING

PHASE I MECHANICAL TEST RESULTS

S. Kaplan

March 8, 1976

Approved by: R G Sim

R. G. Sim
Manager, Core Engineering

AT03-76SF77011

Work Performed Under
United States Energy Research and Development Administration
Contract No. E(04-3)-893
Task 11, 189 No. SG010

General Electric Company
Fast Breeder Reactor Department
Sunnyvale, California

letter dated April 9.

TABLE OF CONTENTS

1.0 SUMMARY

Wire wrap fuel bundle compression tests were performed on 217 rod assemblies in a special test fixture which allowed the determination of the bundle across-flats compression spring constant and fuel rod lateral displacement characteristics. Five bundle configurations were tested; the reference FFTF/CRBR straight start (0°-0°-0°), and four advanced designs selected to provide softer bundle compression characteristics, the straight start with distributed wireless rods, 0°-30°-60° staggered start, 0°-45°-90° staggered start, and the locked-wrap bundle. The relative bundle compression spring constants were determined to be approximately as follows:

straight start (0°-0°-0°)	1.0
0°-0°-0° with distributed wireless	0.2
0°-30°-60° staggered start	0.2
0°-45°-90° staggered start	0.1
locked wrap	0.01

Dispersion of the rod displacements from pinch planes and rod-to-rod nesting displacements in the softened bundles, demonstrated that bundle-to-channel interference considerably in excess of one wire diameter can be accommodated before edge row fuel rods contact the channel wall. The bundle-channel interferences which can be accommodated are approximately as follows:

straight start (0°-0°-0°)	∿ .140 inch (3.6 mm)
0°-0°-0° with distributed wireless 0°-30°-60° staggered start 0°-45°-90° staggered start	∿ .250 inch (6.4 mm)
locked-wrap	>> .250 inch (6.4 mm)

The "wireless" bundle has been identified for near-term development, having exhibited favorable compression characteristics, but particularly for its potential economic incentives. The bundle pressure drop will decrease because approximately 25% of the rods are wireless for 217- and 271-rod assemblies. Because of the bundle simplicity, a minimal degree of assembly and irradiation experience is required for verification of this design.

The locked-wrap bundle has been identified for longer range development. Extremely favorable bundle compression characteristics were exhibited. Prior to irradiation testing, additional work is required to improve the method of bundle assembly and handling and to establish the bundle's hydraulic characteristics.

2.0 INTRODUCTION

2.1 Background and Justification

The objective of the wire-wrap program is to develop a wire-wrap fuel rod assembly capable of meeting LMFBR performance goals. To achieve this, significant effort is being directed towards the investigation of wire-wrap fuel assembly response to relative bundle-to-channel growth and towards the development of advanced assembly designs which will minimize the effect of relative growth on bundle performance during operation.

The wire-wrap assembly of a target LMFBR may be required to operate to a peak burnup of approximately 150,000 MWd/Te and a peak fast fluence of 2.5 to 3.0 x 10^{23} n/cm^2. With the present reference core structural material (316 SS-20% CW), these operating conditions can, as presently predicted, result in significant (up to 30% $\Delta V/V$) irradiation growth of the assembly and significant growth of the fuel rod bundle relative to the channel. This latter phenomenon is of particular importance in the design of the fuel assembly.

Excessive growth of the fuel rod bundle relative to the channel results in a number of potential problems of a design limiting nature, which must be investigated. These include: 1) potentially damaging pinch loads along the channel; 2) inter-bundle dispersion and displacement of the fuel rods resulting in increased cladding hot spot temperatures; and 3) for the case of channel growth relative to bundle, vibration and fretting.

The driving force which eventually results in relative growth is the bundle-to-channel temperature difference. This can be minimized through the use of reduced edge spacing. This reduction in edge spacing has shown excellent promise in analytical studies, both in reducing relative bundle-to-channel growth and in increased fuel rod performance, by reducing the bypass flow around the exterior of the bundle. Since, however, it does reduce the edge clearance, it also limits the amount of overall bundle distortion which can be accommodated. Also to be considered is the fact that the reduction in bundle-to-channel interference is the net result of increased channel growth. This increase must be considered in relation to the design and performance of the core restraint system.

End-of-life loads and bundle interference can be decreased by increasing the amount of as-built porosity. This is a direct method for providing room for relative growth. However, recent in-pile data on 37- and 61-rod assemblies have indicated that an upper limit exists at or near the reference FTR design to preclude excessive fretting. The effects of large clearances on the overall thermal-hydraulic behavior of the assembly are also uncertain with this approach.

The most promising method of reducing the effects of interference is through the use of improved spacing techniques and other bundle assembly advances. The principal advantage of this approach is the ability of an assembly to accommodate swelling internally without the negative aspects of large as-built porosity. It would thus be possible to construct a tight bundle (reduced porosity) for improved vibration control while still providing room for relative growth. Such improved spacing techniques as staggered starts, wireless fuel rods, etc., are being considered.

The bundle-to-channel interference can be simulated in a test fixture where external displacements are applied to the bundle at positions of normal contact between the channel and the bundle. This report summarizes a series of bundle compression tests conducted on a number of advanced fuel assembly designs and compares their performance relative to the reference, straight-start wire-wrap bundle.

2.2 Phase I Compression Test Objectives

Compression tests were conducted on various LMFBR wire-wrapped assemblies to:

1. Determine load and displacement characteristics of the fuel rods to allow accurate analysis of in-pile mechanical and thermal-hydraulic behavior which require knowledge of these characteristics.

2. Determine an optimum design for an LMFBR fuel assembly with respect to accommodation of bundle-channel interference at high fluences and burnup.

3. Determine input data for effective design of hydraulic and irradiation tests.

The bundle configrations tested included the current FTR reference design, which consists of uniform diameter wire, a constant wrap start angle and a 12-inch wire-wrap pitch, and the following variations on this design:

1. Bundle with 55 wireless (non-wrapped) rods
2. 0°-45°-90° staggered wire start angles
3. 0°-30°-60° staggered wire start angles
4. Locked-wrap configuration

These designs are described in Section 4 below.

The following measurements were obtained on each bundle:

1. Displacements at all load pads
2. Loads at load pads, six load pads located in a helical array at the mid-length region of the bundle
3. Individual rod displacements across a characteristic plane of the bundle

3.0 DESCRIPTION OF TEST EQUIPMENT

An elevation view of the test equipment is shown in Figure 1. The test rig is located in the fuel assembly test pit of BTF-III and is rigidly supported on all sides to assure stability between the test rig and the optical displacement equipment located above the compression fixture.

The fixture itself consists of six rigid vertical beams positioned radially around the test bundle in a hexagonal configuration. Each beam is equipped with horizontal borings spaced along its length which provide the locations for the load screw assemblies. An incremental loading generated by rotation of the load screws is transmitted to the bundle through a load pad support system. The load pads provide the same constraints on the bundle as would the actual channel.

Calibrated load cells monitor the force applied by the load screws and dial indicators, located between the beam and the load pad, measure the amount of bundle deflection. The load deflection data then yields the spring constants of the various bundles tested.

Rod dispersion - the geometric distribution and scattering of rods within the channel confine, the spacing between the rods and the spacing between the edge rods and the channel - is measured using the optical displacement equipment incorporated with the test fixture. Relative movement of an axially located target within each dummy fuel rod is monitored using a reflex optical mirror in conjunction with a dual-axis coordinate cathetometer. Illumination of the targets is accomplished by axial diffusion from a single light source located at the bottom of the test assembly.

The repeatability of the measurements was observed to be consistently within $\pm$0.002 inches (.05 mm). Repeatability is the significant instrumentation parameter, as the readings are used only to obtain displacements of each rod, as opposed to determining rod-to-rod measurements. The rod displacements measured between any two degrees of bundle compression are considered accurate to within approximately $\pm$.004 inches (.10 mm) due to possible error accumulation This possible error is independent of the degree of bundle compression and rod displacement.

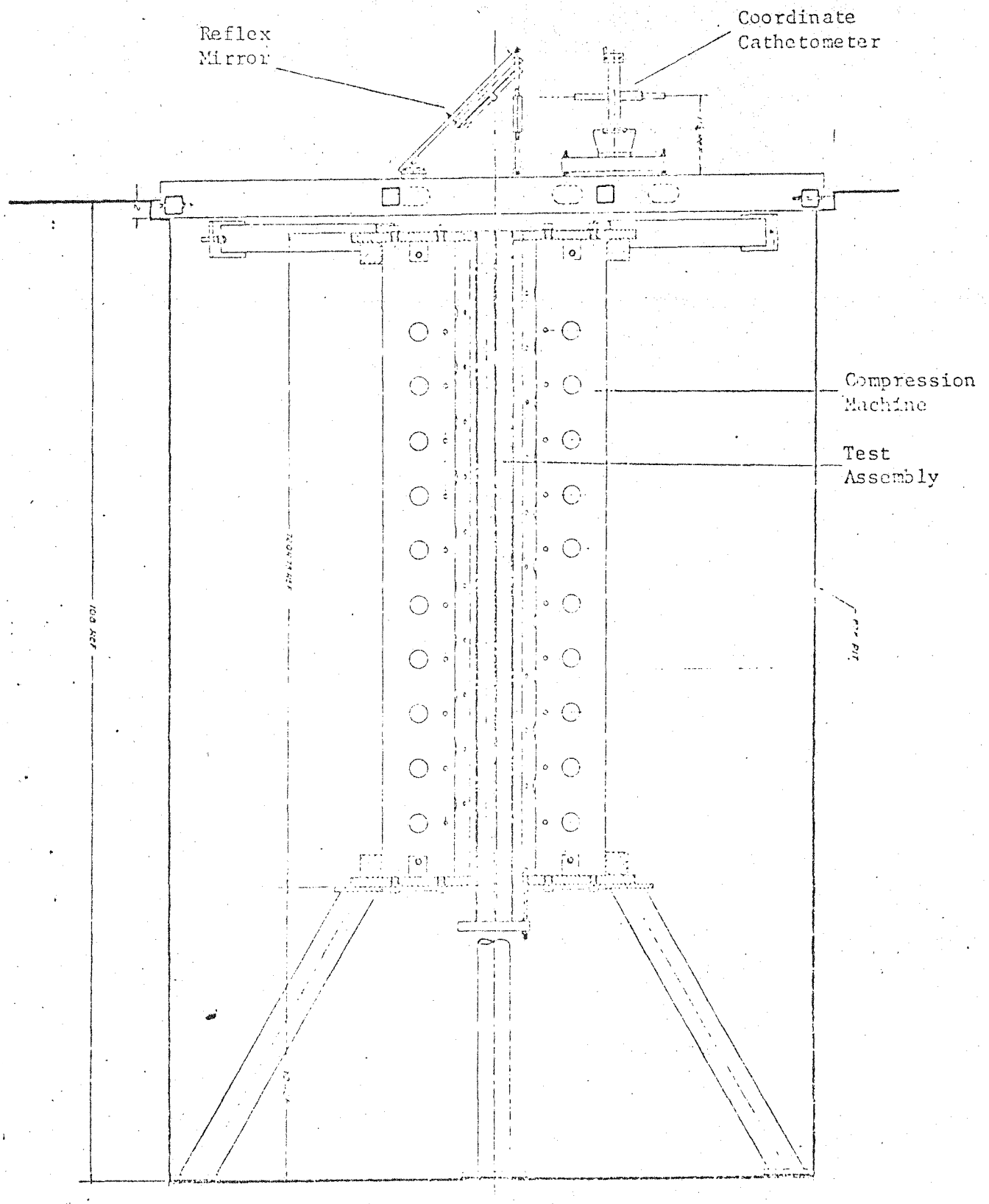

MECHANICAL TEST FIXTURE

FIGURE 1

4.0 DESCRIPTION OF TEST BUNDLES

The completed Phase I test matrix is summarized in Table 1. Tests 1.0 were on the reference, state-of-the-art wire-wrap fuel rod bundle (straight start, CRBR design) and are intended to provide a base reference point for future comparison as well as data on the response of this bundle configuration.

Tests 2.0 are of a straight-start bundle with 55 distributed wireless fuel rods, as illustrated in Figure 2. It should be noted that the pattern has been set in such a way as to insure that no two adjacent rods are wireless, that no edge rods are wireless, and to most effectively disrupt the load path. This wireless array is completely symmetric about all flat-to-flat and corner-to-corner diagonals, resulting in a hexagonal fuel rod bundle with an equal distribution of wireless rods in each of its six triangular segments. Other wireless arrays are conceivable, however, none exhibit the unique properties of the selected wireless array.

Test series 3.0 and 4.0 are tests of staggered start bundles. Two such arrays are included (the 0°-45°-90° and 0°-30°-60°) to confirm and quantify the expected improvements in bundle flexibility predicted with increased relative rotation of the wire wrap start locations.

Tests 5.0 are compression and displacement investigations of the locked-wrap design.

The locked-wrap, 0°-120°-240° staggered start array significantly differs from other staggered-start designs that have considerably less staggering. With previous staggered-start designs the upper bound staggered-start limit was approximately 0°-60°-120°, as greater rotations caused the wires to interfere with each other. Attempting a 0°-120°-240° stagger would cause the wires to interfere with each other in clusters of three, making fabrication with normal wire dimensions impossible. The locked-wrap design reduces the wire diameter so that there is no interference, and the three wires act together

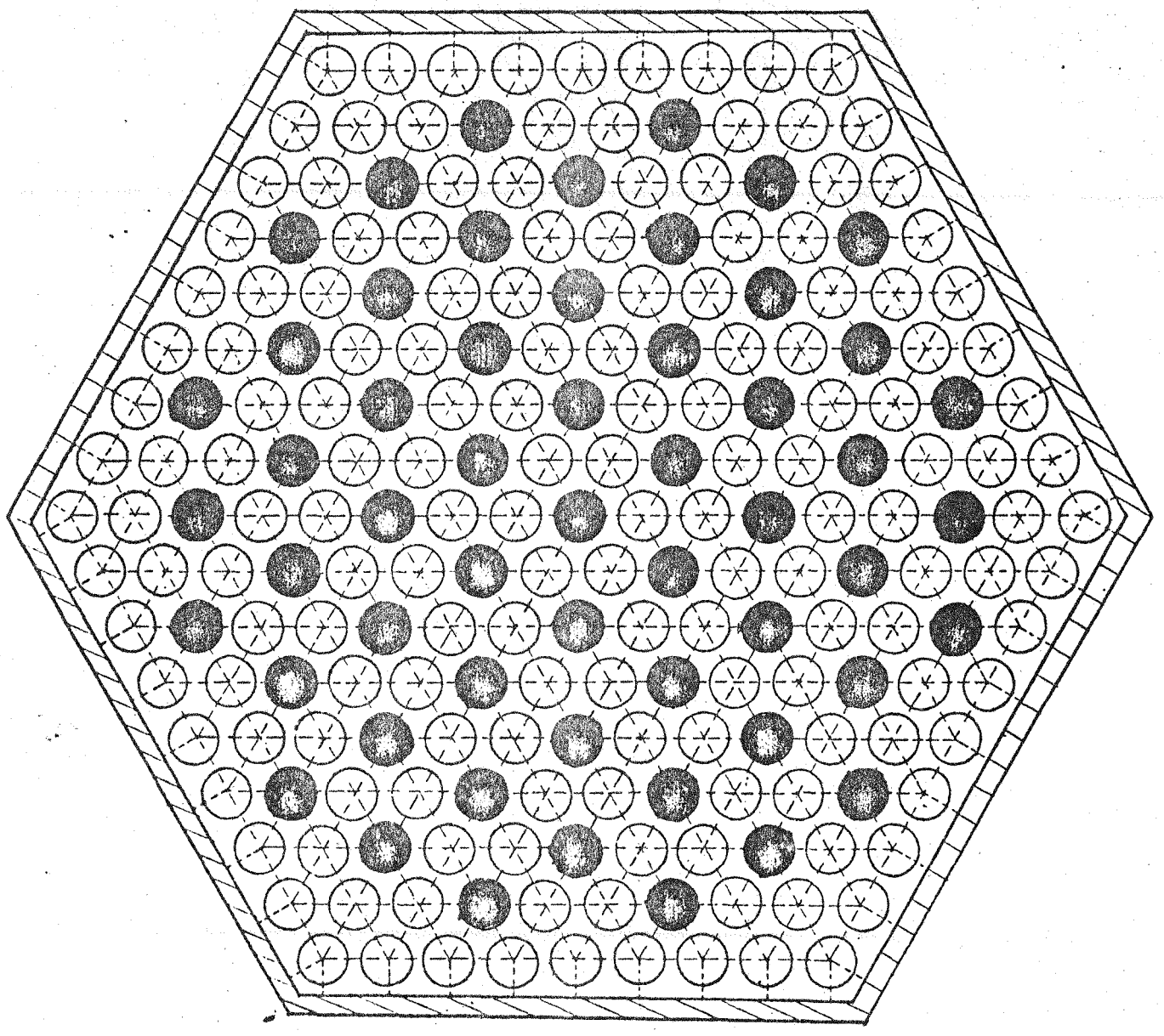

WIRELESS ROD

STRAIGHT START WITH DISTRIBUTED WIRELESS RODS

FIGURE 2

TABLE 1

BUNDLE COMPRESSION AND DISTRIBUTION TESTS

Test Number	Test Conditions	Maximum Expected Mechanical Interaction in. (mm)	Specific Objective of Test
1.0	Straight start (current reference)	0.10 (2.5)	Tc obtain data on current reference design; provide basis for future comparisons
2.0	Bundle with uniformly distributed wireless rods	0.20 (5.0)	To obtain data on rod response and dispersion in softened array
3.0	Bundle with 0°-45°-90° staggered wire-wrap start angles	0.20 (5.0)	To obtain data on response and dispersion in arrays. Softened by wire-wrap staggering
4.0	Bundle with 0°-30°-60° staggered wire-wrap start angles	0.20 (5.0)	
5.0	Locked-wrap bundle, 0°-120°-240° starts	0.20 (5.0)	To obtain data on this unique staggered-start design

to space the rods as desired. See Figure 3. This reduced wire diameter also reduces the edge spacing and channel size for the same rod-to-rod spacing. The manner in which the three wires engage each other tends to lock the rods together at each of the wire cluster locations. As one of the three clustered wires tries to escape the locked position, a section of that wire immediately above or below the locked plane is blocked by the wire of one of the other two rods which pass through the same rod-to-rod clearance flow channel. This extended blockage of a wire from escaping the locked position is readily observed on a model of the configuration.

The locked-wrap design has a number of inherent advantages over other designs. These are:

1. The contact between rods is a wire-to-wire contact. This prevents point loading on the rods; instead the load will be distributed along a helical line. This is preferred for bundle-to-channel differential expansion-induced contact loads. However, it may be far more significant in terms of fretting and wear considerations of the fuel rods which are caused by sliding, rolling, or impacting between a cladding surface and a neighboring fuel rod's wire wrapper. Most (conceivably all) of the fretting and wear may be restricted to wires only.

2. There is a reduction in the steel volume fraction compared to conventional wire-wrap spacing designs. This is because a smaller wire diameter is required to produce the same rod-to-rod spacing.

3. With the smaller wire-wrap diameter, a reduction in edge spacing occurs reducing edge coolant bypass flow and thereby improving the overall bundle thermal-hydraulic performance.

A patent disclosure (GE No. 24-AD-B4049) describing this unique wire-wrap design in detail has been prepared and submitted to GE and US-ERDA legal service organizations.

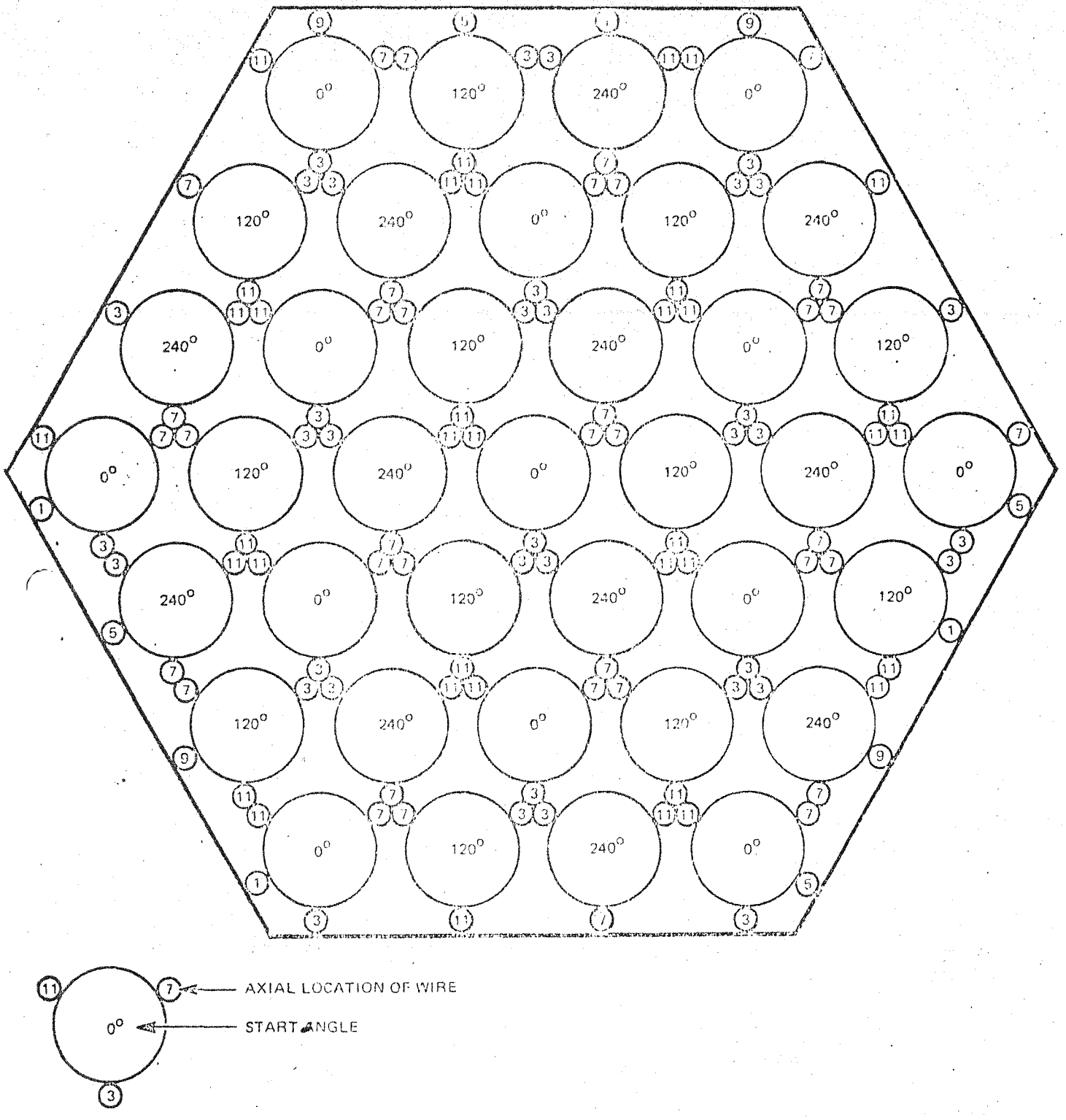

Figure 3. Locked-Wrap Design Wire Contact Locations

All bundles use the CRBR rod dimensions, that is, 0.230 inch (5.84 mm) diameter cladding and 0.056 inch (1.42 mm) diameter wire, except for the locked-wrap bundle which uses 0.0465 inch (1.18 mm) diameter wire to achieve the same rod-to-rod spacing of 0.286 inch (7.26 mm).

5.0 TEST RESULTS

As presented in Table I, it was originally anticipated that approximately .10 inches (2.54 mm) across-flats compression would be applied to the straight start test and approximately .20 inches (5.08 mm) cross-flats compression would be applied to the various softened bundles. The straight start test was terminated at .070 inch (1.78 mm) bundle compression, as a predetermined limit of approximately 500 pounds (226.8 kg) per load pad was reached. This limit was determined to assure that no local permanent set would be imposed on the rods. The softened bundles, with the exception of the locked wrap bundle, were loaded to approximately .160 inch (4.06 mm) interference. This limit was selected when it was observed that optical data would be somewhat limited beyond this compression due to rod bending displacements. The locked wrap bundle was compressed to approximately a .210 inch (5.34 mm) interference. The corresponding across-flats dimension represented the limiting testing machine compression as limited by load pad bridging.

5.1 Bundle Load-Compression Characteristics

Due to "shakedown" problems involving the operation of the compression testing machine and its instrumentation, the first test on the straight-start bundle was performed four times, tests 1.1.1, 1.1.2, 1.1.3, and 1.1.4. Of these four tests, the load vs. across-the-flats displacement measurements (i.e., bundle compression spring constant data) were measured for tests 1.1.2, 1.1.3, and 1.1.4. The data for the displacements of the rods, which were optically measured across a plane at approximately the bundle mid-height and at the same elevation as a loading pad, are available only for test 1.1.4.

Figure 4 shows the load-bundle compression displacement data. The data points represent the average load calculated from six load cells located in a helical array about the approximate mid-length of the bundle. Initially it was planned to load the bundle with approximately 0.100 inches (2.54 mm) across-the-flat compression, anticipating a load of approximately 450 to 500 pounds (204 to 227 kg) per load pad to attain that degree of compression. The limit was set at a load of approximately 50 to 60 pounds (22.7 to 27.2 kg) per rod (nine edge rods are loaded by each load pad) so as to have ample margin against local permanent deformation of a rod. The anticipated load-displacement

was based on the predicted stiffness using the semi-empirical equation of Reference 1.

$$W = 129 \frac{EI \frac{N}{6}}{p^3} \Delta \text{ or } K = \frac{129\ EI \frac{N}{6}}{p^3}$$

where

W = load per side per pitch, pound
K = spring constant, pound per pitch per inch
E = modulus of elasticity, psi
I = rod moment of inertia, $in.^4$
N = number of fuel rods
P = wire-wrap pitch, inch
Δ = flat-to-flat compression, inc.

where the factor 6, alternately referred to as C_D the dispersion coefficient, is an experimentally determined constant based on tests on 37-, 127-, and 217-rod bundles. This equation resulted in a predicted spring constant of 4486 pounds per pitch length per inch (80.1 kg per mm) of across-the-flats compression.

As shown in Figure 4, the load is not linear with displacement; rather it can be approximated by a bilinear curve. In the range of 4.280 inches (108.71 mm) to 4.22 inches (107.19 mm) across-the-flats dimension (the nominal tight bundle being 4.301 inches (109.24 mm)), a spring constant of 8730 pounds per pitch length per inch (155.9 kg per mm) occurs, which is approximately double the predicted spring constant.

The semi-empirical expression for the bundle across-flats compression stiffness was developed using test data reported from Reference 2 for bundle-to-channel interaction testing of a 217-rod FFTF prototype assembly. Figure 5 shows the test data as reported in Reference 2 with the current GE test data superimposed. The current data closely approximates the earlier data over the low compression range. However, for higher degree of bundle-to-channel interaction, the bundle stiffens by approximately a factor of two.

STRAIGHT START (0°-0°-0°)

COMPRESSION DATA

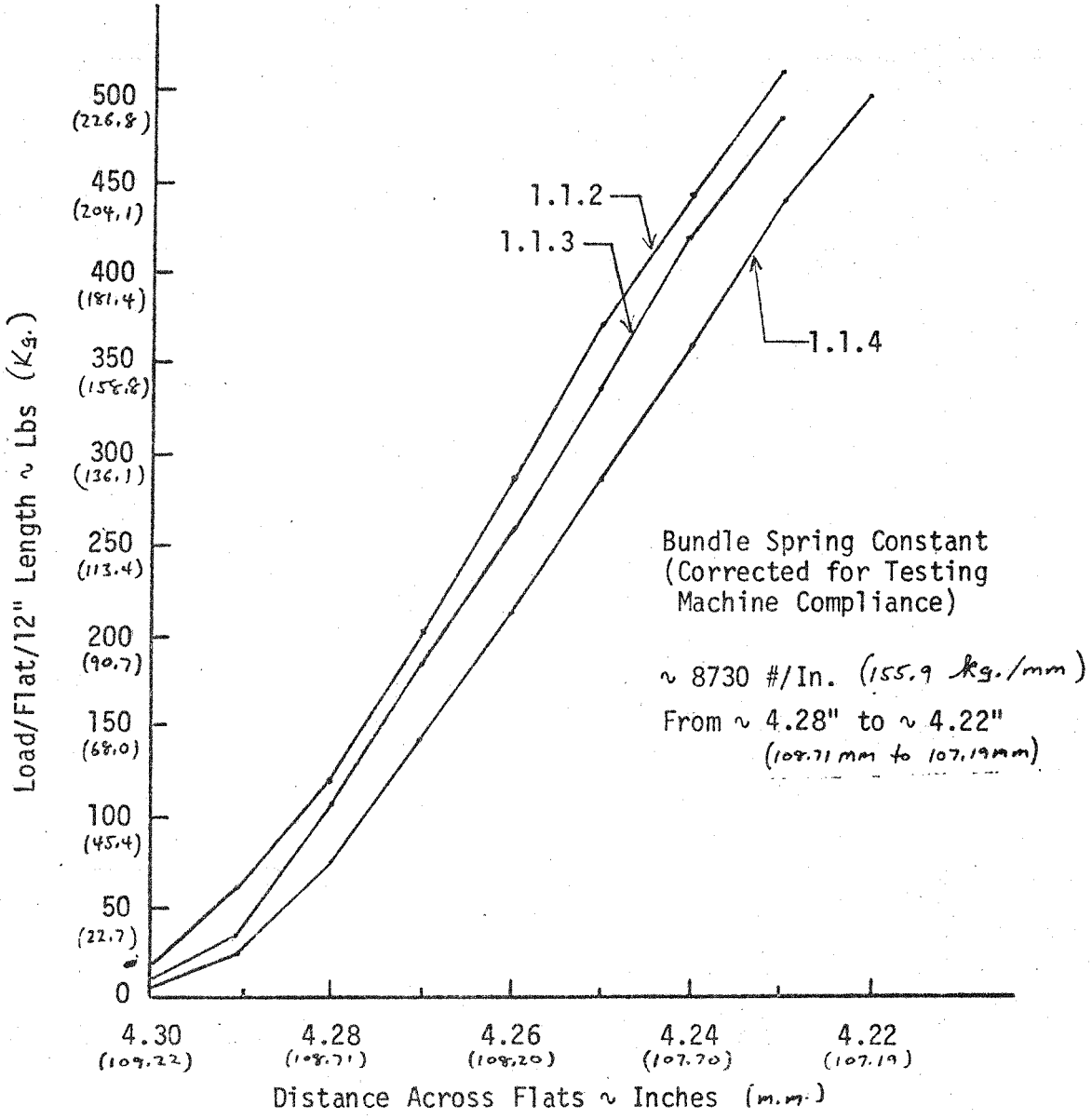

FIGURE 4

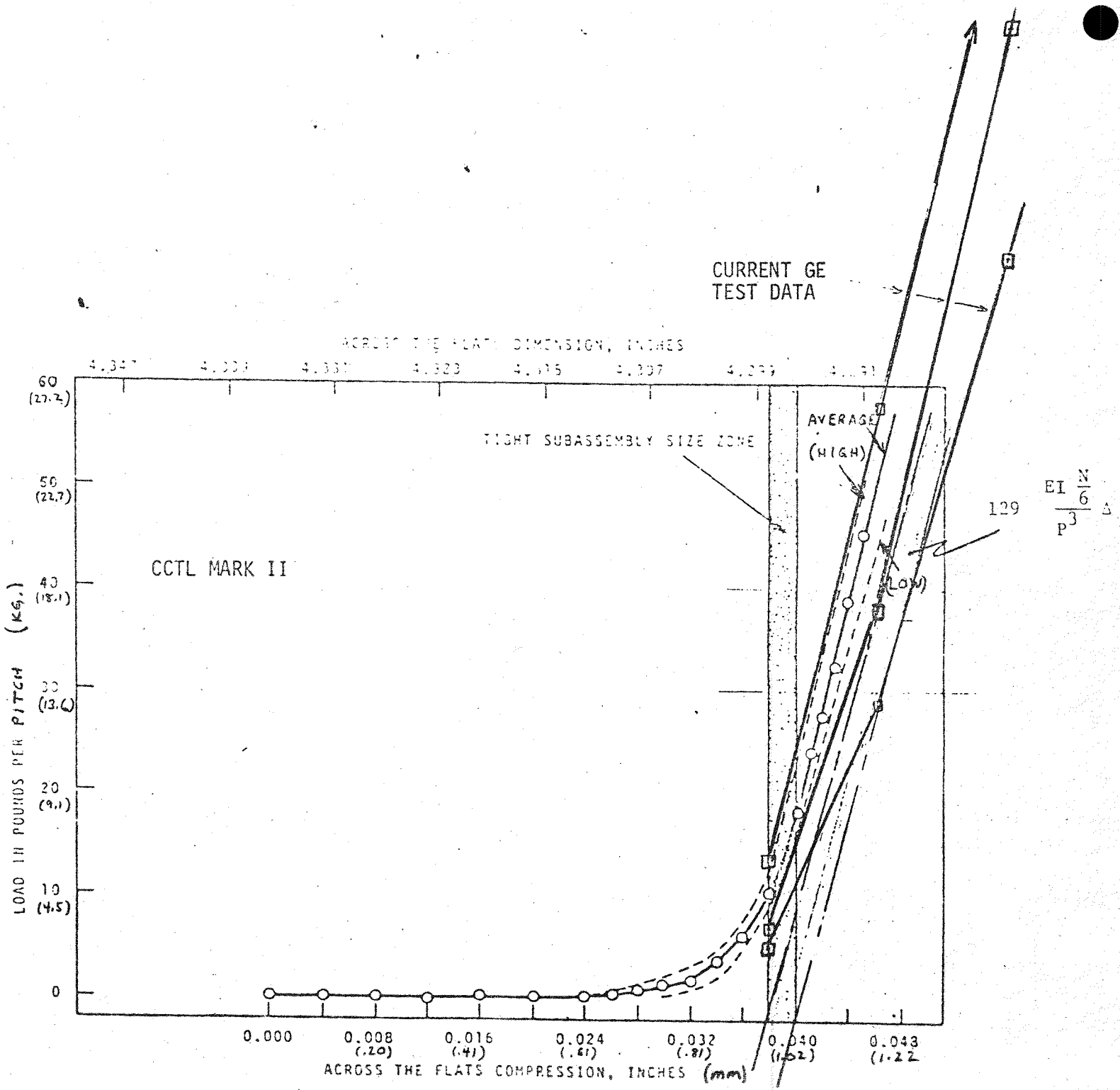

Figure 5 Comparison of Current Data with Early HEDL Data for Low Range Compression

Figure 6 shows load-displacement data for the various bundle configurations tested, the data being the average compression measured in the six hex flats. As in Figure 4, the data include the compliance of the test fixture, which adds .002 inch (0.5 mm) of across-flats displacement for each 100 pounds (45.4 kg). Thus, for example, of the .160 inch (1.06 mm) across-the-flats compression for the 0°-30°-60° staggered-start bundle which occurred at approximately 300 pounds (136.08 kg), .006 inch (.15 mm) is caused by the test fixture compliance and .154 inch (3.91 mm) is due to bundle compression. Similarly, for the straight-start bundle, .010 inch (25 mm) of the .080 inch (2.03 mm) displacement is due to the test fixture compliance and .070 inch (1.78 mm) is the bundle across-flats compression displacement.

The stiffness of the 0°-30°-60° staggered start and the wireless bundle are both approximately 20% that of the straight start. The 0°-45°-90° staggered-start bundle is approximately half as stiff as the 0°-30°-60° and the wireless bundles. The locked wrap bundle is two orders of magnitude less stiff than the constant start bundle. The approximations to the relative bundle stiffnesses are being considered pending further interpretation of the data. No explanation is apparent for either the sudden change in the compression characteristics of the wireless bundle or the manner in which all bundles display greater flexibility in the low compression range.

The 0°-45°-90° bundle was compressed twice, with the test designated 3.1.1 (not shown in Figure 6) being terminated at approximately .070 inch (1.78 mm) compression beyond the tight bundle dimensions. The test was terminated as it was observed that an edge rod was rotated 180° from its proper position. The bundle was disassembled and the assembly error corrected. All other rods were observed to have been properly positioned. The load-displacement data for the two compression tests on the 0°-45°-90° bundle are shown in Figure 7 over the displacement range obtained for test 3.1.1. The closeness of the curves lends confidence to the repeatability of the results.

5.2 Interpretation of Rod Displacement Data

Before presenting the rod displacement measurements, it is useful to discuss the manner in which the test data are to be interpreted for in-reactor and

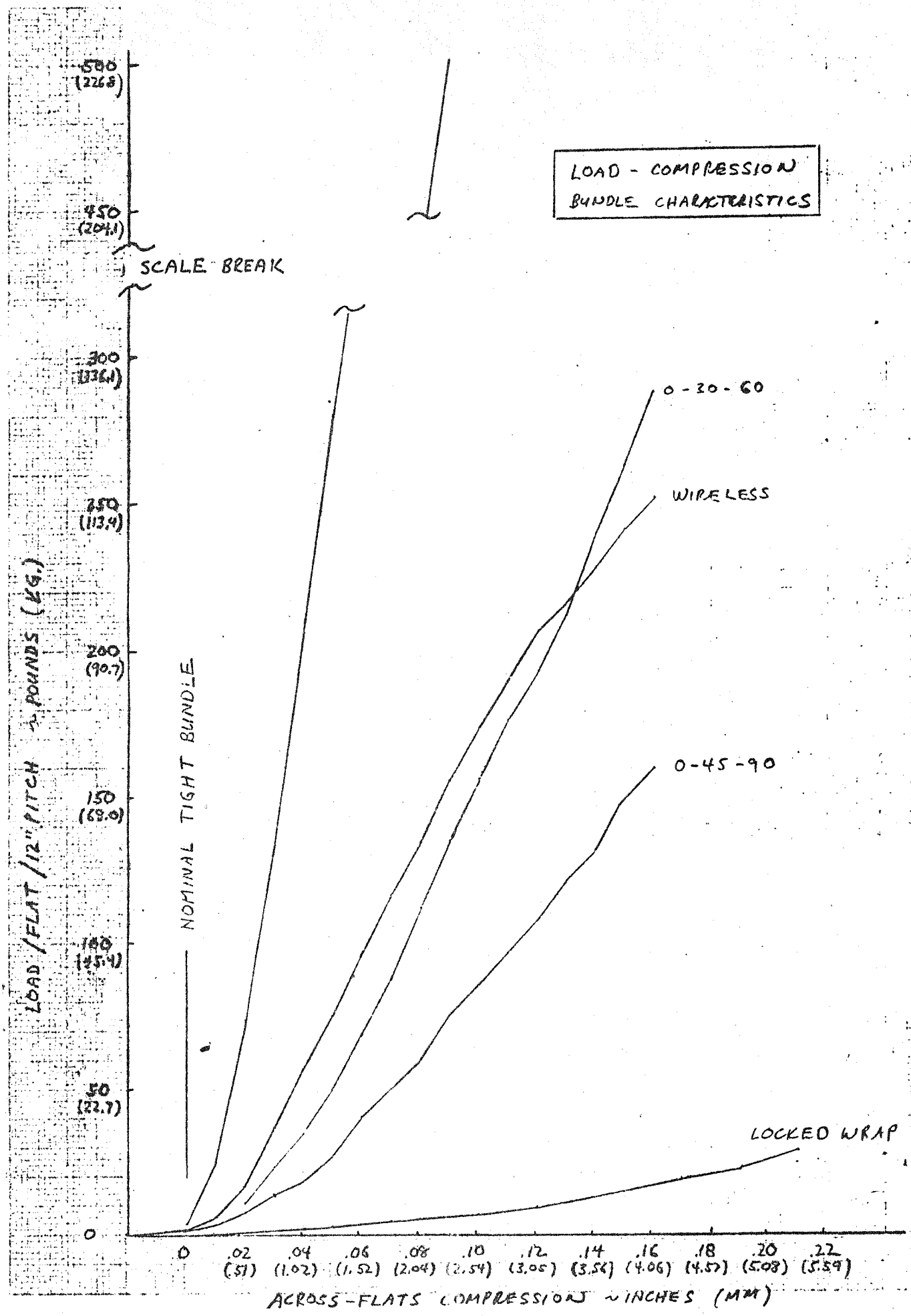
LOAD - COMPRESSION
BUNDLE CHARACTERISTICS
500 (226.8)
450 (204.1)
SCALE BREAK
300 (136.1)
250 (113.4)
200 (90.7)
150 (68.0)
100 (45.4)
50 (22.7)
0
LOAD / FLAT / 12" PITCH - POUNDS (KG.)
NOMINAL TIGHT BUNDLE
0-20-60
WIRELESS
0-45-90
LOCKED WRAP
0
.02 (.51)
.04 (1.02)
.06 (1.52)
.08 (2.04)
.10 (2.54)
.12 (3.05)
.14 (3.56)
.16 (4.06)
.18 (4.57)
.20 (5.08)
.22 (5.59)
ACROSS-FLATS COMPRESSION - INCHES (MM)

FIGURE 6

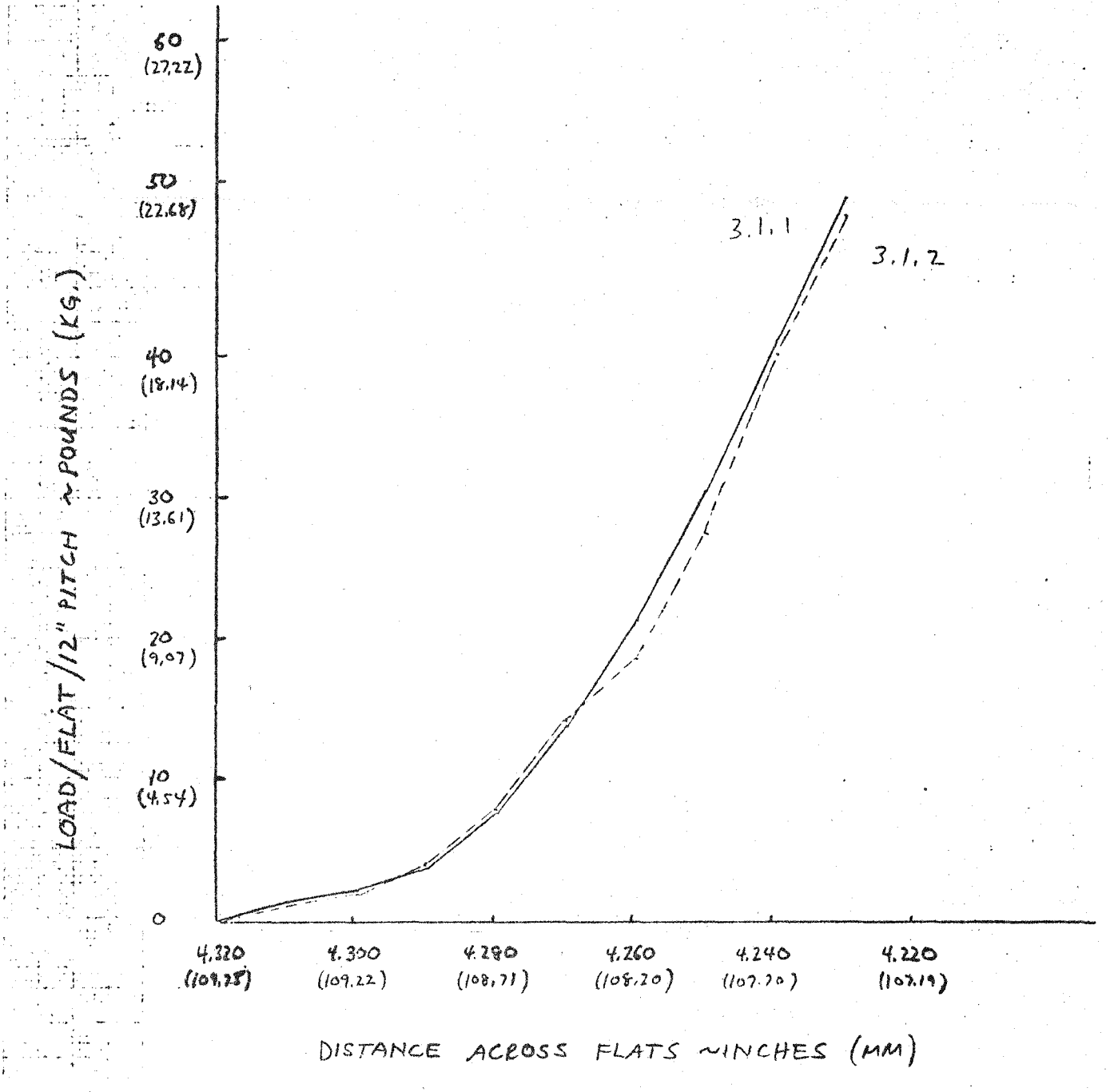

COMPRESSION TESTS ON 0°-45°-90° BUNDLE

FIGURE 7

mechanical test characteristics is that, for in-reactor behavior, the bundle-to-channel differential growth is generated by restraining the bundle radial displacement to zero at the helical array of locations where the bundle is spaced from the channel by the wire wrappings; whereas the test fixture imposes a radial displacement at these same locations.

Figure 8a shows that the initial and final positions of the load pads impose, in a helical manner, a radial displacement of one-half of the across-flats compression. The load pads simulate the portion of the fuel assembly channel which contacts the bundle wires along the edges. Figure 8b shows the bundle cross section at a load plane, the plane at which the edge wires contact the "10 o'clock" hex flat, assuming that the bundle deflects in a helical manner with no dispersion. (Dispersion is defined as internal rod-to-rod displacement mechanisms which distort the bundle cross section and result in decreasing the bundle outer across-flats dimension.) The difference between the load pad inner envelope in Figure 8a and the compressed bundle envelope in Figure 8b represents the relative motion at the plane between the edge rods and the channel of the in-reactor bundle. Thus at the 10 o'clock flat where the wires space the bundle at that plane, no relative motion occurs between the bundle and channel. At the opposite (4 o'clock) flat, the relative displacement between the bundle and the channel is $\delta_{A/F}$ (i.e., $.5\ \delta_{A/F} + .5\delta_{A/F}$). At this plane the 4 o'clock hex flat is located midway between the two planes at which the wires space this flat of the bundle from the channel. For a wire diameter of .056 inch (1.42 mm) (FFTF and CRBR), when the bundle-to-channel differential growth exceeds .056 inch (1.42 mm) across-flats (after the initial bundle assembly clearance is closed due to differential growth) the bundle will contact the channel at this location if no dispersion occurs. If dispersion occurs, as shown in Figure 8c, the relative bundle-to-channel displacements for the in-reactor condition are found by the difference between the inner envelope of the pads at the compressed bundle as shown in Figure 8a and the compressed bundle envelope as shown in Figure 8b. Thus for a .056 inch (1.42 mm) diameter wire spacer, the bundle will contact the channel when

$$0.5\ \delta_{A/F} - \overline{\delta} \geq 0.056$$

where $\overline{\delta}$ is positive as shown in Figure 8c.

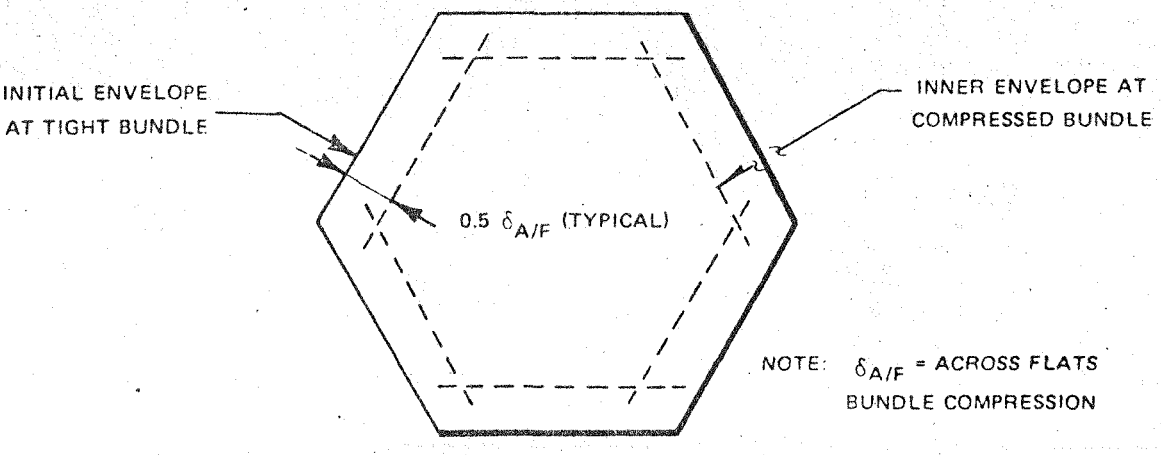

(a) LOAD PAD ENVELOPES

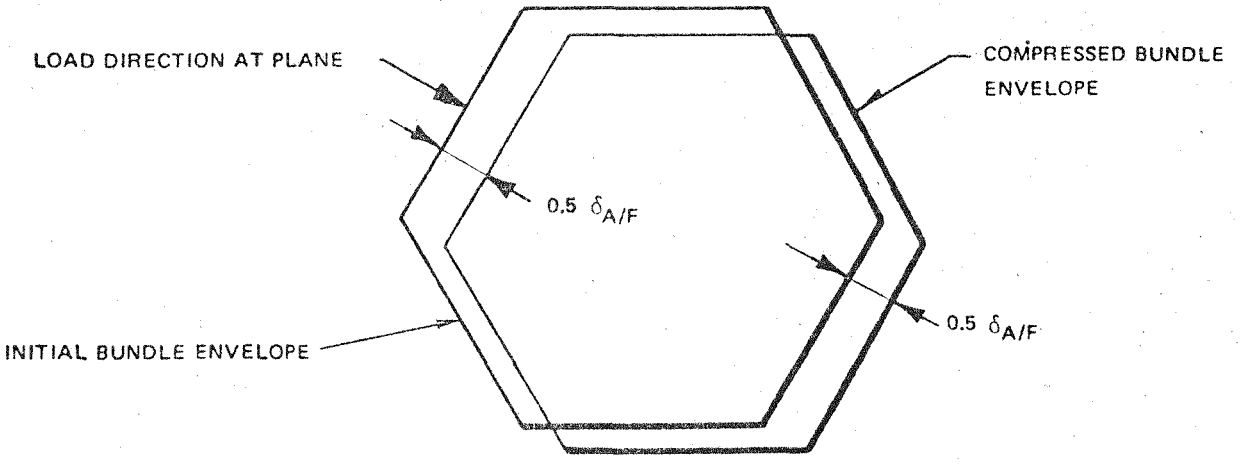

(b) BUNDLE DISPLACEMENT AT PLANE, NO DISPERSION

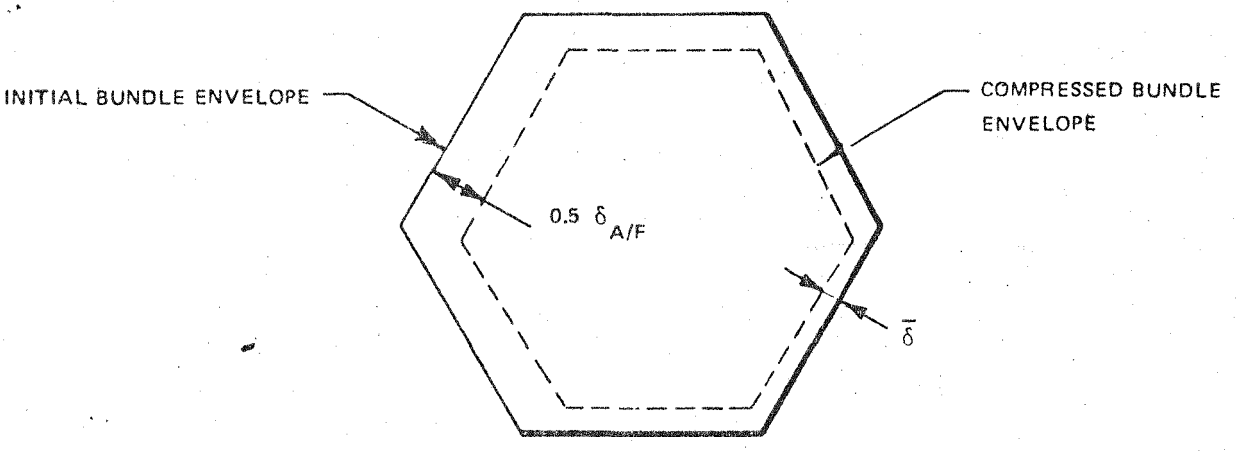

(c) BUNDLE DISPLACEMENT AT PLANE, DISPERSION

Test Bundle Compression Characteristics

FIGURE 8

Rod-to-rod clearance data for the in-reactor bundle-channel interference which is being modeled in the compression test is directly obtained from the compression test as the relative rod-to-rod centerline displacement data. In order to obtain the in-reactor rod-to-rod centerline displacements from the compression test data, the radially integrated bundle swelling plus thermal expansion (minus that of the channel) must be added to those from the compression test. For example, consider a hypothetical bundle spaced such it behaves in a homogeneous manner. As a more visual example, consider the bundle to be a plane consisting of 217 rigid rings with each ring radially spaced from its neighbors by radial springs. When subjected to bundle-to-channel interaction, the in-reactor version of the bundle will result in no relative motion of the ring centers, but clearance between rings will be diminished by the combination of ring radial growth and spring radial compression. The test fixture version of the bundle will have displacement of the ring centers toward the bundle center and rod-to-rod clearance decreases, with the latter being the same as for the in-reactor bundle.

5.3 Rod Displacements

Figure 9 is a computer-generated output of the rod displacements for the straight-start (0°-0°-0°) bundle at an across-flats compression of .070 inch (1.78 mm). (The nominal applied compression was .080 inch (2.03 mm), however, .010 inch is due to test fixture compliance.) The plot is constructed by the computer output "printing" a 217-rod array designated by + characters and simultaneously printing * characters at vector-determined positions for the displacements. The + and * are connected by hand and the + characters are circled for clarity. The magnitude of the displacement vectors can be approximated by considering that the rods along the 10 o'clock hex edge have components normal to the edge of approximately .5 $\delta_{A/F}$, .035 inch (.89 mm). The spacings between adjacent rods, which are a different linear scale, are approximately .286 inch (7.26 mm). At 21 locations, indicated by darkened rings, no optical targets were available and the data shown in Figure 8 for these locations are obtained by interpolation. The effect of the dispersion mechanism is apparent as evidenced by the varied magnitude of the displacements and the manner in which the 4 o'clock flat displaces inward rather than approximately .035 inch (.89 mm) outward.

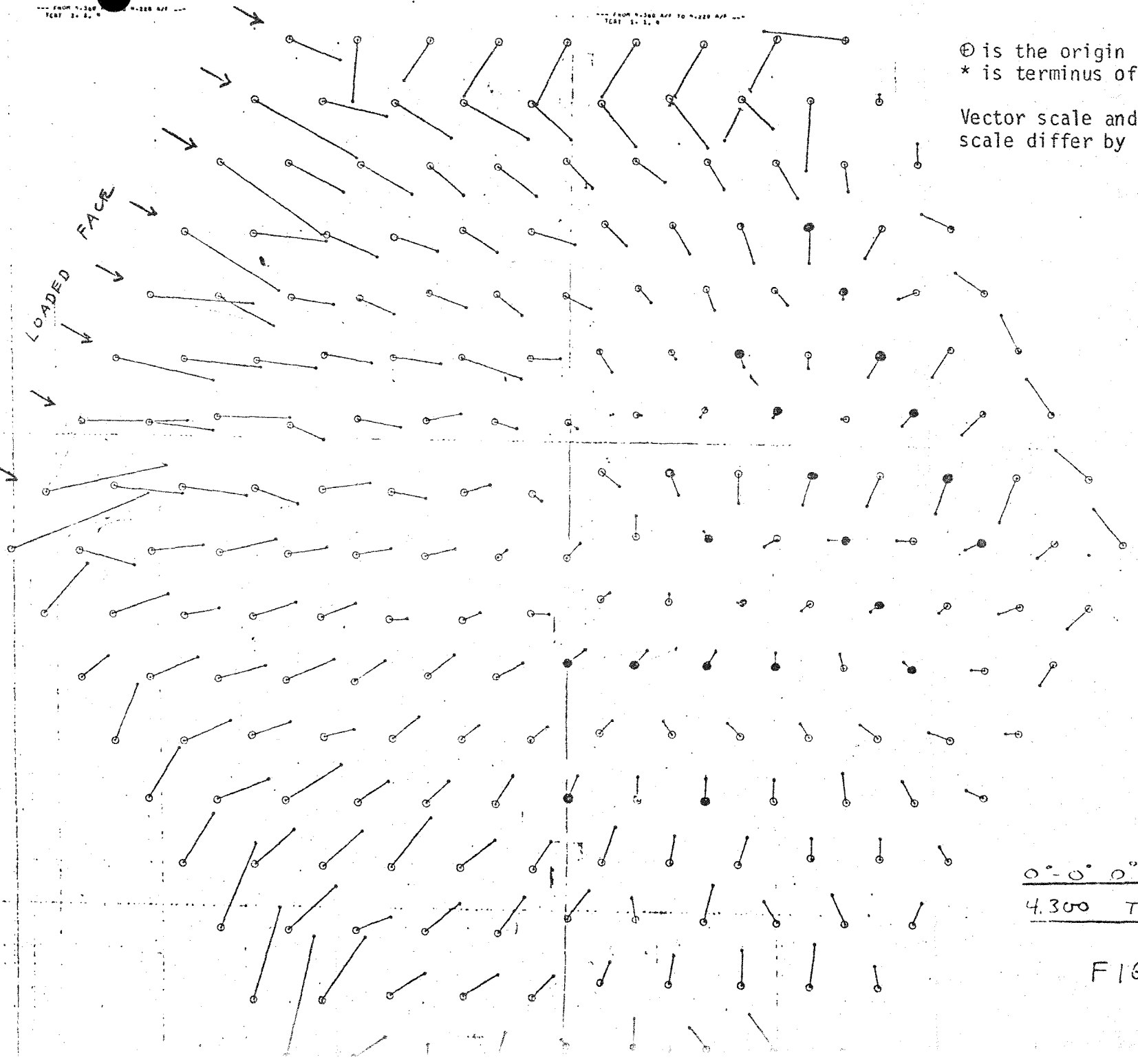

⊕ is the origin of displacement vect
* is terminus of displacement vector.

Vector scale and rod original positic
scale differ by an order of magnitude

0°-0° 0° DISPLACEMENTS
4.300 TO 4.230 A/F

FIGURE 9

From Figure 9 some general observations are apparent. It is noted that the corner rods displace erratically compared to the other rods. This erratic behavior is believed to occur over the entire bundle axial length based on observations made, while the bundle was compressed, along the complete outer "surface" of the bundle. The erratic displacements are associated with movement of the wire wrap. This movement occurs even though the wires are pretensioned according to typical FTR/CRBR specifications. (Between tests the bundles were disassembled and the wires were manually adjusted to return the rods to as-fabricated condition. No wire "loosening" was detected. It is believed that all rods were in a newly fabricated condition prior to each test.) The corner rods at 9 and 11 o'clock, which were in contact with the load pad at the plane shown in Figure 9, should both exhibit approximately .035 inch (.89 mm) displacements normal to the 10 o'clock hex edge. The variance in the 11 o'clock rod is probably due to the wire contact shifting. Similarly the 1 o'clock corner rod, which displaces very erractically, may reflect wire movement at above and/or below wire-to-load-pad contact. In fact it appears that the displacement of this rod may be associated with, or may be the cause of, the unpredictable displacements all along the 2 o'clock hex flat.

It should also be considered that at the corner rods the nonprototypical feature of the testing fixture, whereby the load pads move into the bundle rather than the bundle bearing out radially against a fixed position boundary could result in a rod sliding laterially. Ideally this should not occur due the manner in which the corner rod is cradles in the corner. However, considering that the load pads are displaced individually rather than simultaneously, and considering that the sometimes erratic nature of friction may be a factor, may explain the observed behavior.

Another general observation is an apparent row-to-row nesting mechanism occurring at the rows in the vicinity of wire-to-pad contact, i.e., the 10 o'clock flat where a pad occurs, and the 8 and 12 o'clock flats where the pads are 2 inches (50.8 mm) above and below the plane of Figure 9.

Considering the discussion earlier with respect to Figure 8, and using that as a basis to approximate the bundle-to-channel contact which would occur

at the 4 o'clock hex flat, it is calculated that for the .070 inch (1.78 mm) across-flats bundle-to-channel interference, the bundle maintains a minimum clearance from the channel of approximately .025 inches (.64 mm) for a .056 inch (1.42 mm) diameter wire spacer.

The nature of the displacements of Figure 9 as well as limited visual observation of all edge and corner rods for the length of the bundle leads to the conclusion that variations will occur from plane to plane and test to test. This variation is expected to be greater for the constant start where dispersion results from an unstable loading along pinch planes than for softened bundles where the more stable nesting mechanism is present.

A further discussion of rod displacements is provided in Section 6 where a comparison of rod-to-rod displacement data is made among several bundle designs.

Figure 10 shows the displacements for the 0°-45°-90° staggered-start bundle configuration. The across-flats bundle displacement is .069 inch (1.75 mm) .070 inch (1.78 mm) nominal, with the .001 inch (.02 mm) being in the test fixture. All the rods had optical targets and all displacements represent direct test data. A scale can be approximated for the displacement vectors by considering that the radial displacements along the 10 o'clock flat are approximately .035 inch (.89 mm).

The 45° rods contact the load pads at the optical target level, with the 0° and 90° rods contacting the load pads 1.5 inches (38 mm) above and below the displacement plane. The greater uniformity of the inward radial edge rod displacements is the direct result of the bundle softening mechanism provided by rod-to-rod nesting in conjunction with rod deflections induced by the staggered starts. Considering the discussion earlier with respect to Figure 8, and using that as a basis to approximate the bundle-to-channel contact which would occur at the 4 o'clock hex flat, it is calculated that for the .069 inch (1.75 mm) across-flats bundle-to-channel interference, the bundle maintains a minimum clearance from the channel of approximately .040 inch (1.02 mm) for an .056 inch (1.42 mm) diameter wire-wrap spacer.

Figure 11 shows the displacements for the 0°-30°-60° staggered start bundle configuration. The across-flats bundle displacement is .068 inch (1.73 mm), .070 inch (1.78 mm) nominal minus the .002 inch (.05 mm) deflection of the

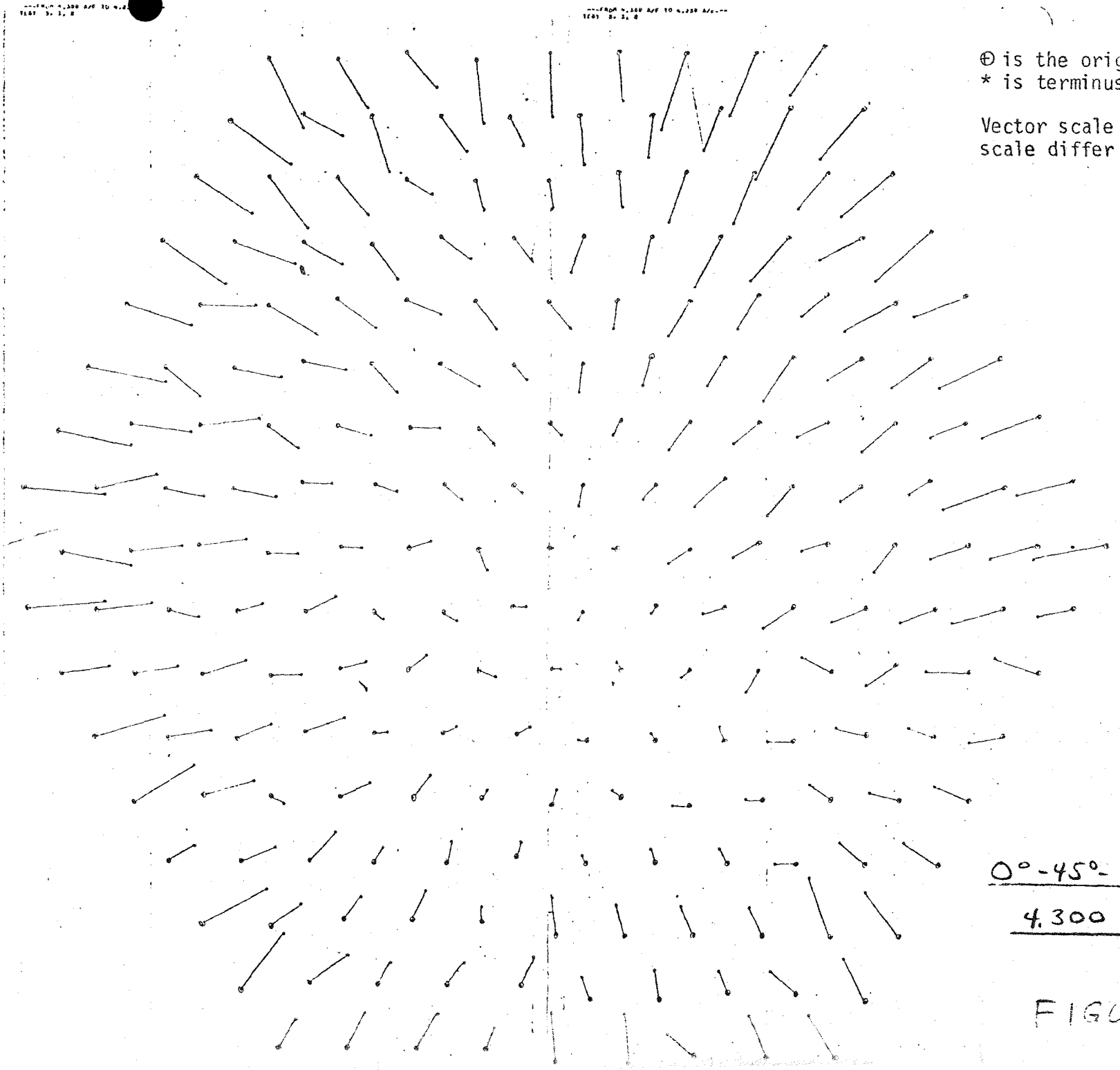

⊕ is the origin of displacement vector.
* is terminus of displacement vector.

Vector scale and rod original position scale differ by an order of magnitude.

0°-45°-90° DISPLACEMENT
4.300 TO 4.230 A/F

FIGURE 10

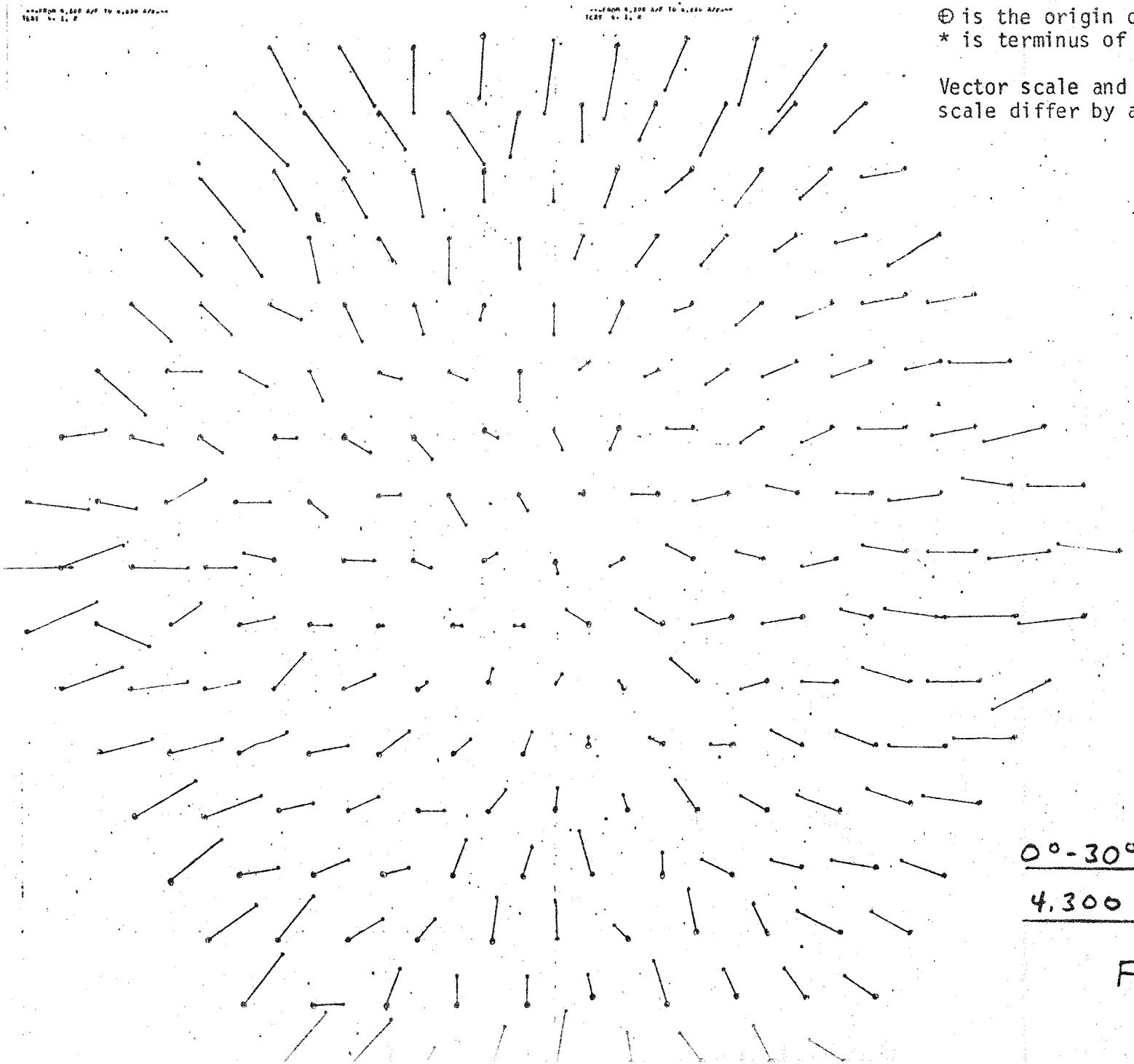

⊕ is the origin of displacement vector.
* is terminus of displacement vector.

Vector scale and rod original position scale differ by an order of magnitude.

0°-30°-60° DISPLACEMENTS

4.300 TO 4.230 A/F

FIGURE 11

test fixture. The 30° rods contact the load pads at the optical target level, with the 0° and 60° rods contacting the load pads 1.0 inches (25 mm) above and below the displacement plane. The greater uniformity of the inward radial edge rod displacements is the direct result of the bundle softening mechanism provided by rod-to-rod nesting in conjunction with rod deflections induced by the staggered starts. Considering the discussion earlier with respect to Figure 8, and using that as a basis to approximate the bundle-to-channel contact which would occur at the 4 o'clock hex flat, it is calculated that for the .068 inch (1.73 mm) across-flats bundle-to-channel interference, the bundle maintains a minimum clearance from the channel of approximately .040 inch (1.02 mm) for an .056 inch (1.42 mm) diameter wire-wrap spacer.

Figure 12 shows the displacements of the straight-start bundle softened by 55 wireless rods (indicated by bold circles). The greater uniformity of the inward radial edge rod displacements is the direct result of the bundle softening mechanism provided by rod-to-rod nesting in conjunction with rod bending induced by the disruptions to the straight start pinch plane. For the .068 inch (1.73 mm) across-flats bundle-to-channel interference the bundle maintains a minimum clearance from the channel of approximately .040 inch (1.02 mm) for a .056 inch (1.42 mm) diameter wire-wrap spacer.

Further discussions of rod displacements is provided in Section 6 where a comparison of rod-to-rod displacement data is made among several bundle designs. Included is the presentation of displacement results for a bundle across-flats compression of approximately .155 inches (3.94 mm) for the softened bundles.

Figure 13 shows the displacements of the locked wrap bundle. The maximum degree of wire wrap staggering, 0°-120°-240°, results in near similar loading on all hex flats. The schematic bundle depicted in Figure 3 shows that the 2,6, and 10 o'clock hex flats are identical with respect to rod-to-channel contact locations, as are, also, the 4,8, and 12 o'clock hex flats. At the target level of the bundle, contact between the edge rod wire and the loading pad occurs at three rods on each flat of the 2,6 and 10 o'clock group. Thus

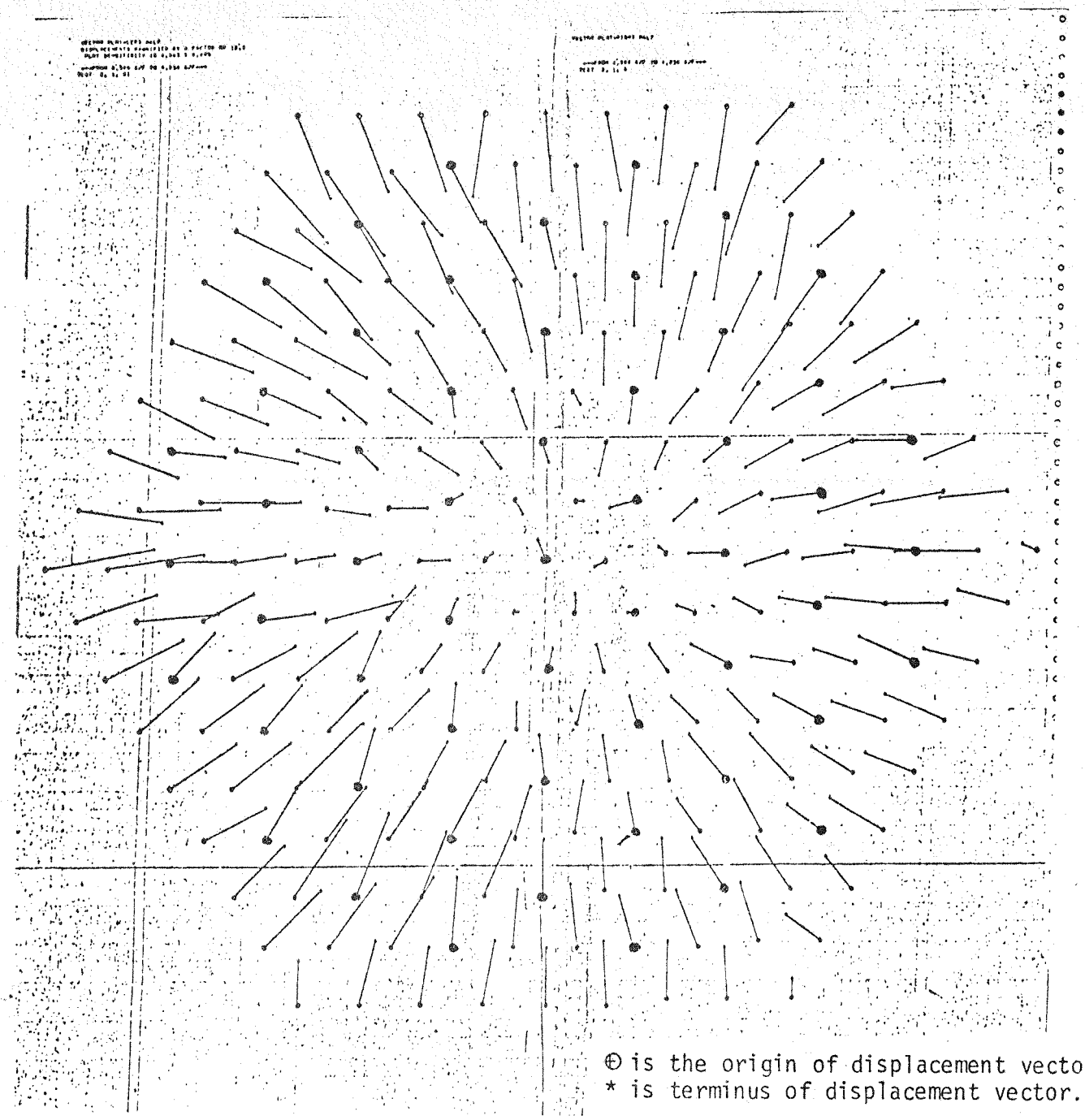

⊕ is the origin of displacement vector.
* is terminus of displacement vector.

Vector scale and rod original position scale differ by an order of magnitude.

DISPLACEMENTS OF 0°-0°-0° WITH WIRELESS RODS, 4.300 TO 4.230 A/F

FIGURE 12

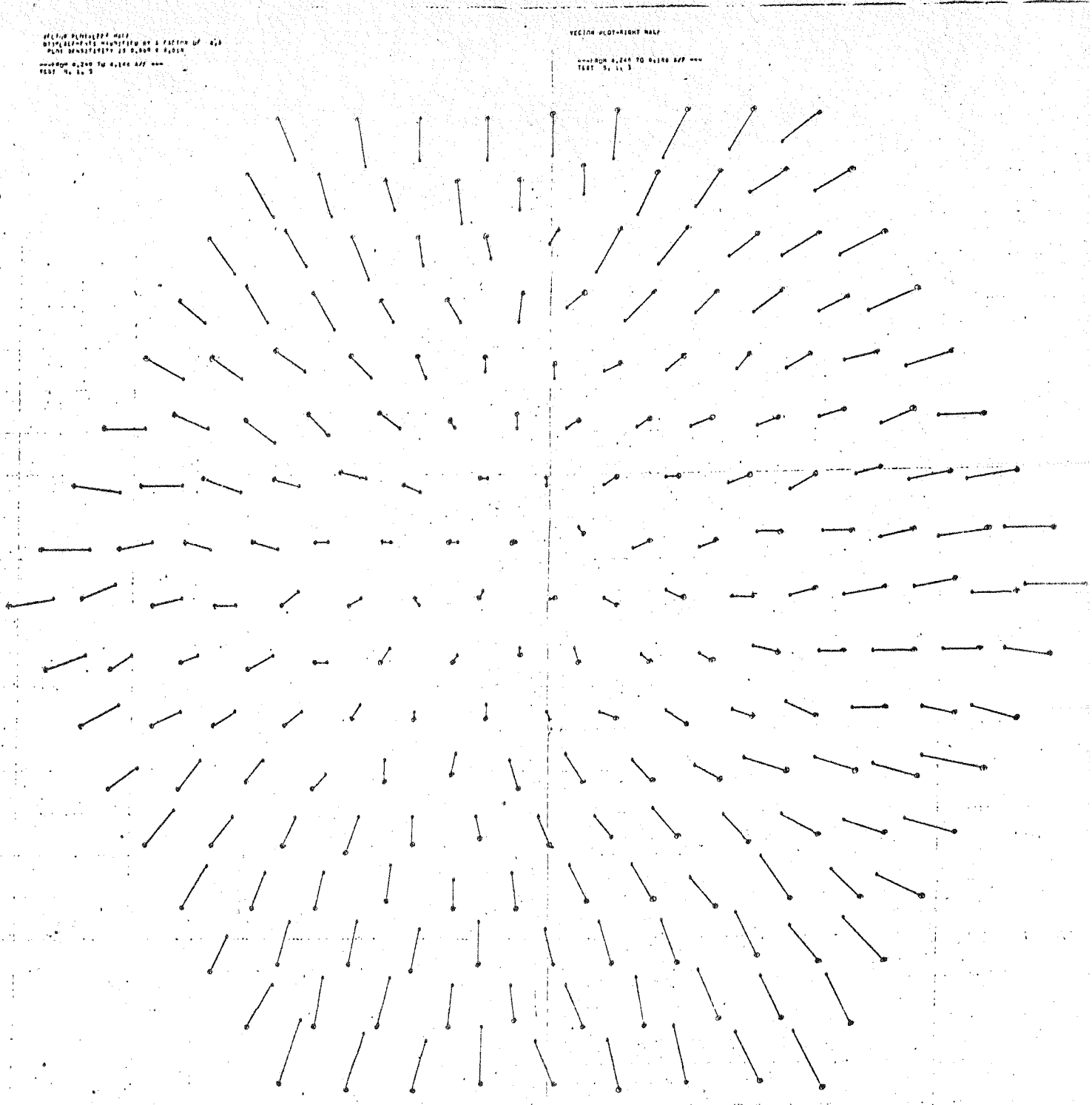

⊕ is the origin of displacement vector.
* is terminus of displacement vector.

Vector scale and rod original position scale differ by an order of magnitude.

LOCKED WRAP DISPLACEMENTS
4,240 TO 4,140 A/F

FIGURE 13

these nine rods will have normal-to-the-flat displacements equal to one-half of the across flats compression. At all other edge rods, the displacement measurements are made at either 2, 4, or 6 inches (50.8, 101.6, or 152.4 mm) from the loading pad contact. To quantitatively determine the decrease in the edge rod-to-channel clearance, the difference in displacements from the edge is calculated between the rods being contacted at the target level and those being contacted 6 inches (152.4 mm) from the target level. Qualitatively it can be seen in Figure 13 that the difference is small relative to the magnitude of the edge rod displacements. This small difference is obscured somewhat due to the round-offs used in the plotting routine. The results for Figure 13 are for an across flats bundle compression of .100 inches (2.54 mm) which has been applied to the bundle after an initial bundle across-flats compression of .030 inches (0.76 mm) had been applied to the bundle. Thus Figure 13 represents displacements occurring as the bundle is compressed from an initial compression of .030 inches (0.76 mm) to a compression of .130 inches (3.30 mm). For the .100 inch (2.54 mm) across-flats bundle-to-channel interference, the bundle maintains a minimum clearance from the channel of approximately .038 inches (0.97 mm) for a .046 inch (1.17 mm) diameter wire. This is consistent with the value obtained by considering the rod helical bending displacements which lead to the rod-to-rod nesting. Based on that consideration, the maximum deflection of an edge rod into the bundle-to-channel edge clearance occurring mid-way between wire-to-channel contact, should be approximately equal to the across-flats compression divided by the number of rows in the bundle, i.e., .100 inches (2.54 mm) divided by 17 rows.

A further discussion of locked wrap bundle rod displacements is provided in Section 6 where a comparison is discussed among several bundle designs, and in Section 7 where a discussion is presented of the handling and testing of the locked wrap design. That discussion assesses the effect of handling problems encountered with the locked wrap bundle and discusses the advantages and the potential problems associated with the design as observed through handling and from the test data.

5.4 Verification of Optical System

For the straight-start test, a partial verification of the optical system capability was attempted by physically measuring the edge rod displacement

components normal to the hex flats. This was done by measuring the distance between the bundle and the test fixture vertical beams as shown in Figure 14. Tight bundle and compressed bundle measurements were made using the telescoping gage and a micrometer. The difference, corrected by .005 inch (.13 mm) deflection of the test fixture beam, are shown in Figure 15. The procedure is difficult as the operator must "feel" the displacement while holding the gage at a proper attitude. Particular difficulty is encountered at the 8 o'clock and 12 o'clock faces where the wire spacers traverse the rod near the measurement location. Comparison of the results with the vector-indicated displacements of Figure 8 provides confirmation that the optical system measurement technique is reliable.

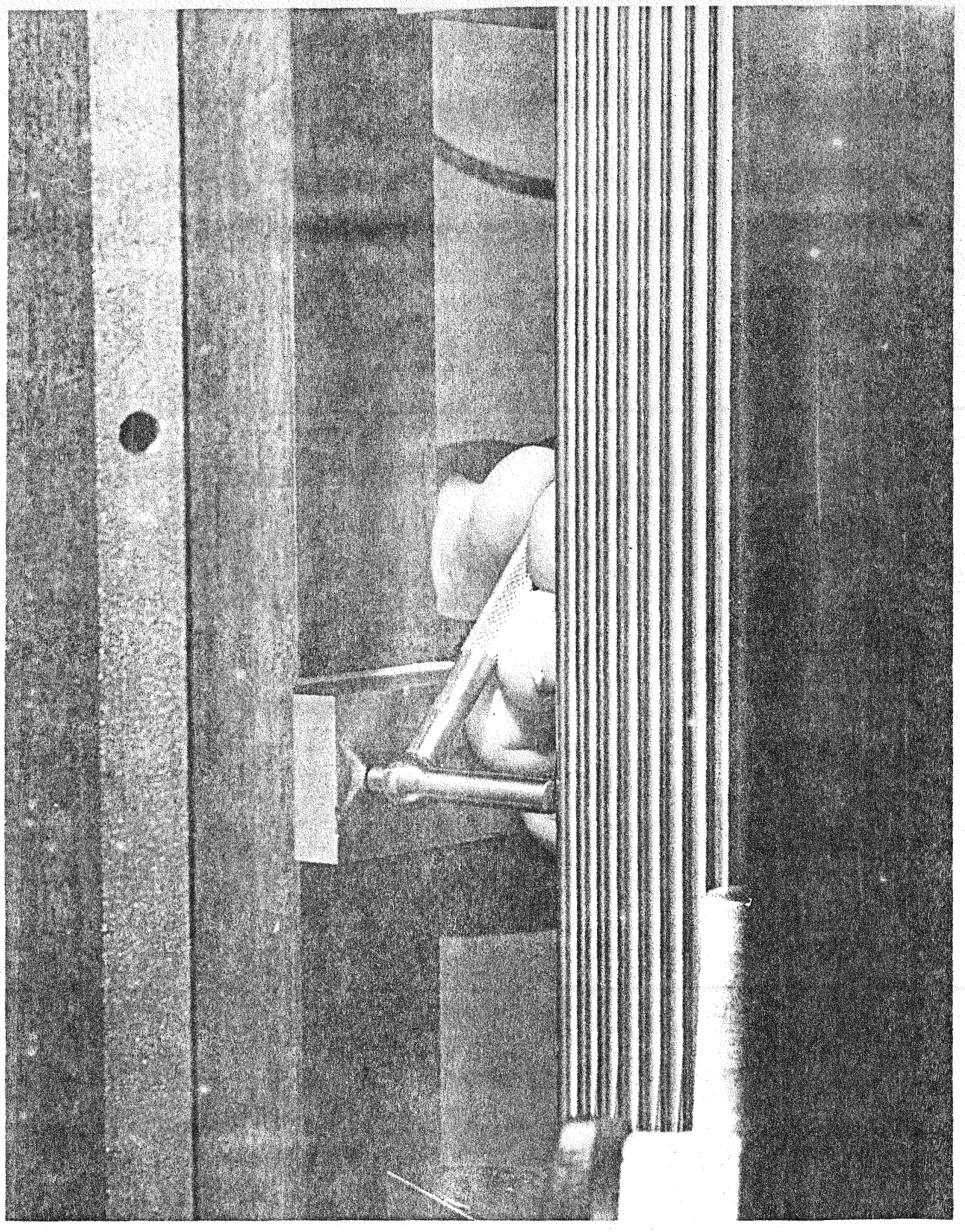

Figure 14 Hand Measurements of Bundle Edge Rod Locations

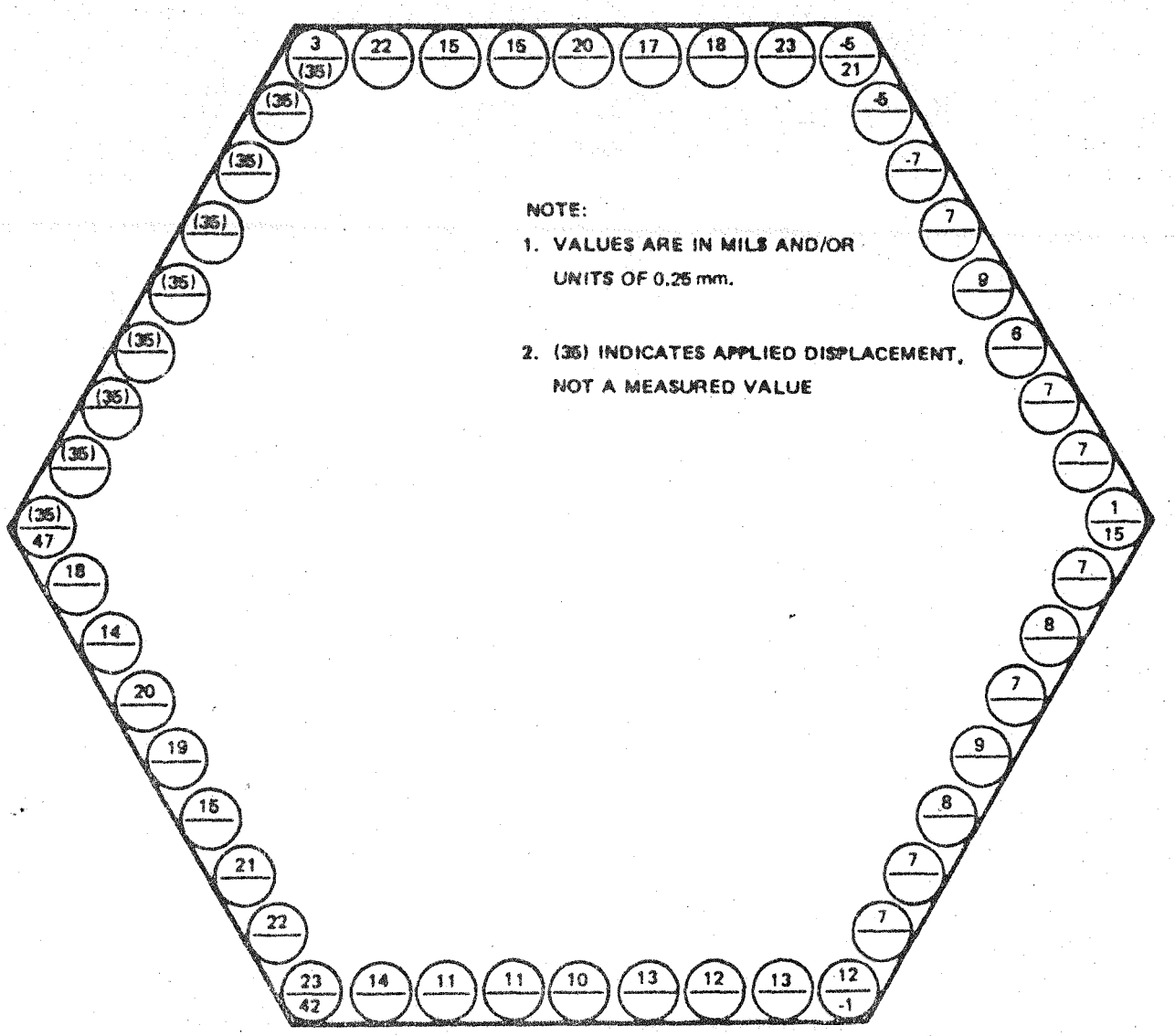

Hand Measurements of Bundle Edge Rod Normal Displacement

FIGURE 15

6.0 COMPARISONS OF BUNDLE DESIGNS

Comparing the data for the various bundle designs, it appears that, for static contact load and rod displacement considerations, the softened bundles provide superior characteristics compared to the reference straight start. The significantly lower contact loads and superior bundle-to-channel spacing are readily observed. Less apparent is the observation that the softened bundles provide superiod rod-to-rod clearances than occurs for the straight start bundle.

The locked wrap bundle design test data demonstrated the desirable mechanical characteristics anticipated at the time of its inception: extreme softness, relatively uniform rod-to-rod spacing variation, and a relatively low decrease of the bundle-to-channel edge clearance. Experience gained during the handling and testing of this assembly indicates that further development is necessary. This is discussed further in Section 7.

Of the other three softened bundles tested, the straight start softened by wireless rods is preferred. This bundle showed favorable characteristics during the mechanical testing, however its choice as an advanced wire-wrapped spacer design is primarily based on its potential overall plant operation economic incentives: bundle assembly simplicity, a bundle pressure drop decrease of 10 to 15% associated with approximately 25% of the rods being wireless, and a slight gain in breeding ratio associated with the slight decrease in steel volume. Furthermore, in-reactor test verification can be approached in a conservative "boot strapping" manner in that the bundle need not be committed in its entirety, but that irradiations can progress from using a limited number of wireless rods to the maximum possible. Of the two staggered start bundles, the softer 0°-45°-90° bundle displayed somewhat superior displacement characteristics than the 0°-30°-60°. A more in-depth comparison between the two bundle arrays or an assessment of staggering that lies between the two arrays has at this time been precluded by the preference for the bundle with distributed wireless rods.

Figures 16,17,18 and 19 schematically show the relative rod-to-rod displacements for the straight start, the straight start with wireless rods, the 0°-45°-90°

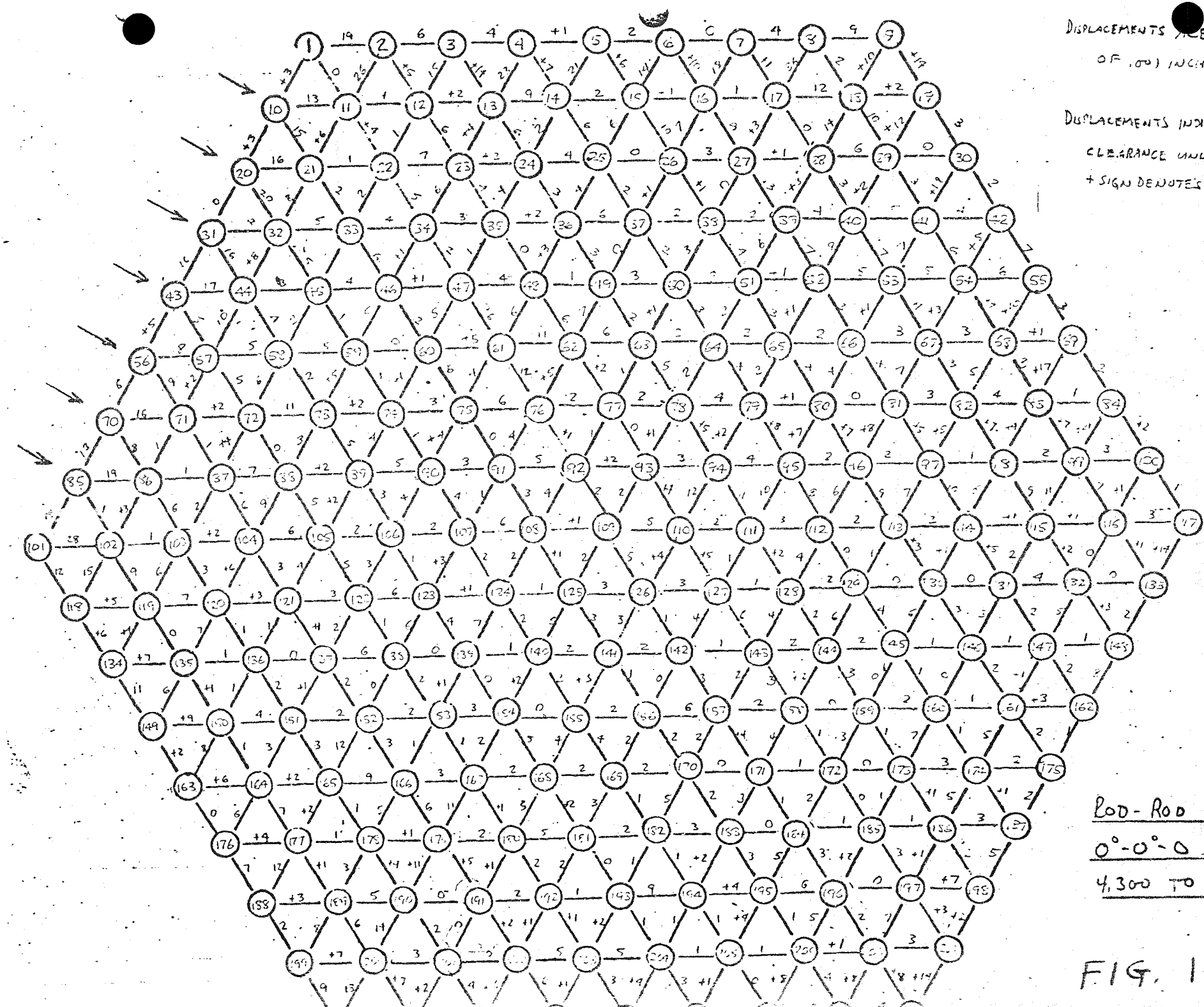

DISPLACEMENTS ARE IN UNITS OF .001 INCH (.0254MM.)

DISPLACEMENTS INDICATE DECREASE CLEARANCE UNLESS + SIGN + SIGN DENOTES INCREASE.

ROD-ROD DISPLACME.

0°-0°-0 BUNDLE

4,300 TO 4,230 #/F

FIG. 16

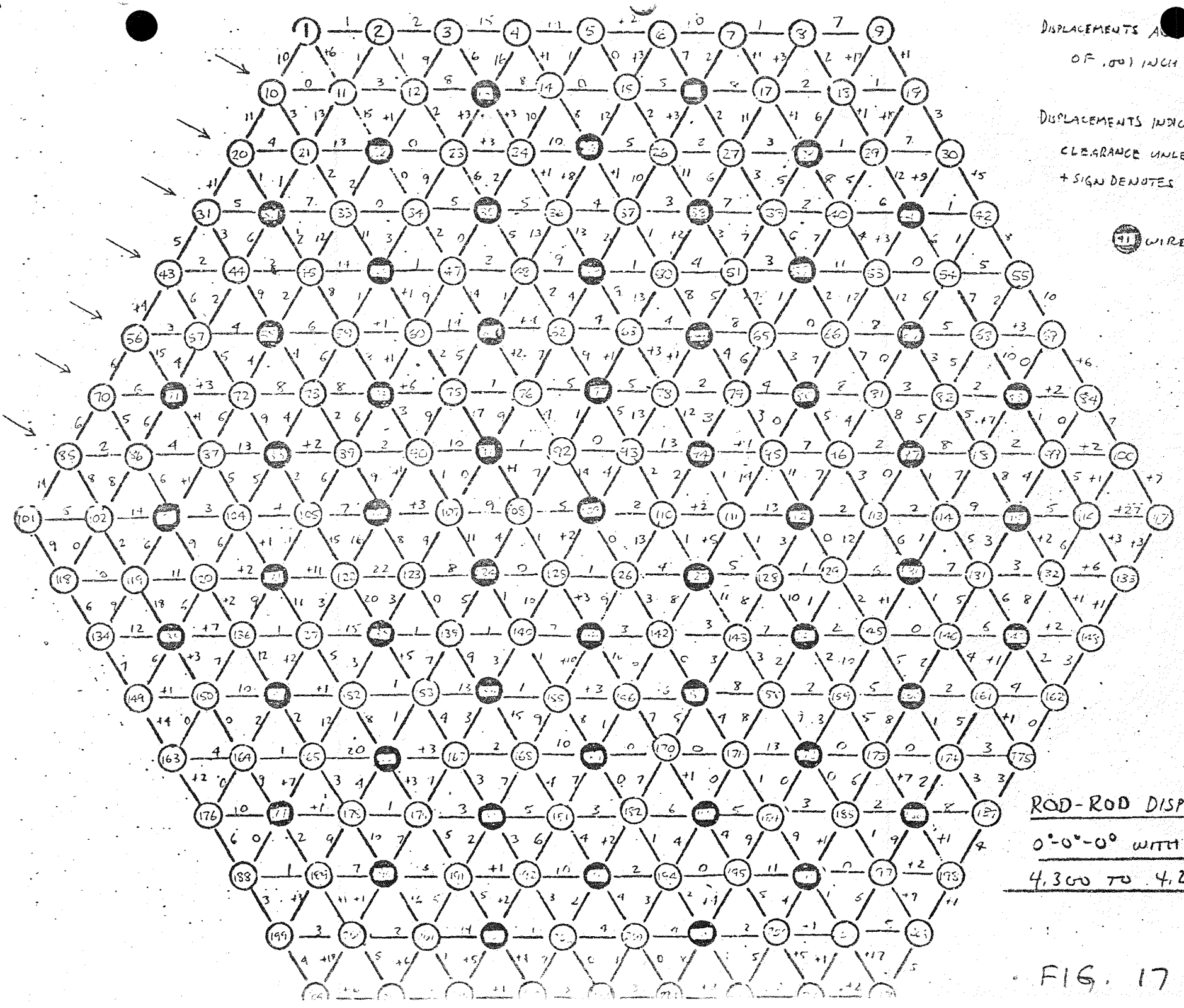

DISPLACEMENTS ARE IN UNITS OF .001 INCH (.0254 MM.)

DISPLACEMENTS INDICATE DECREASED CLEARANCE UNLESS + SIGN. + SIGN DENOTES INCREASE.

91 WIRELESS ROD

ROD-ROD DISPLACEMENT
0°-0°-0° WITH WIRELESS
4,300 TO 4,230 A/F

FIG. 17

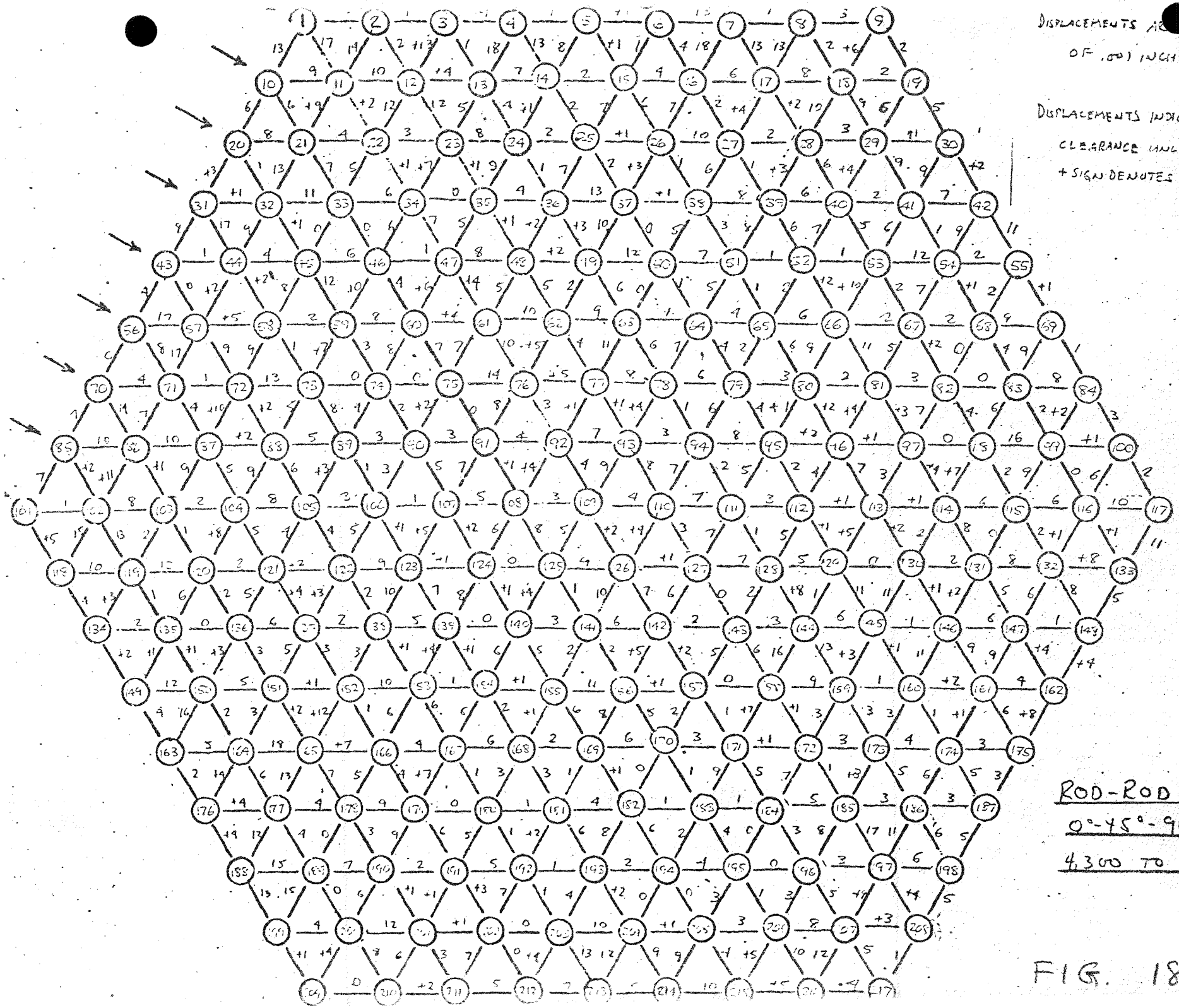

DISPLACEMENTS ARE IN UNITS OF .001 INCH (.0254 MM.)

DISPLACEMENTS INDICATE DECREASED CLEARANCE UNLESS + SIGN. + SIGN DENOTES INCREASE.

ROD-ROD DISPLACEMT.
0°-45°-90° BUNDLE
4.300 TO 4.230 A/F

FIG. 18

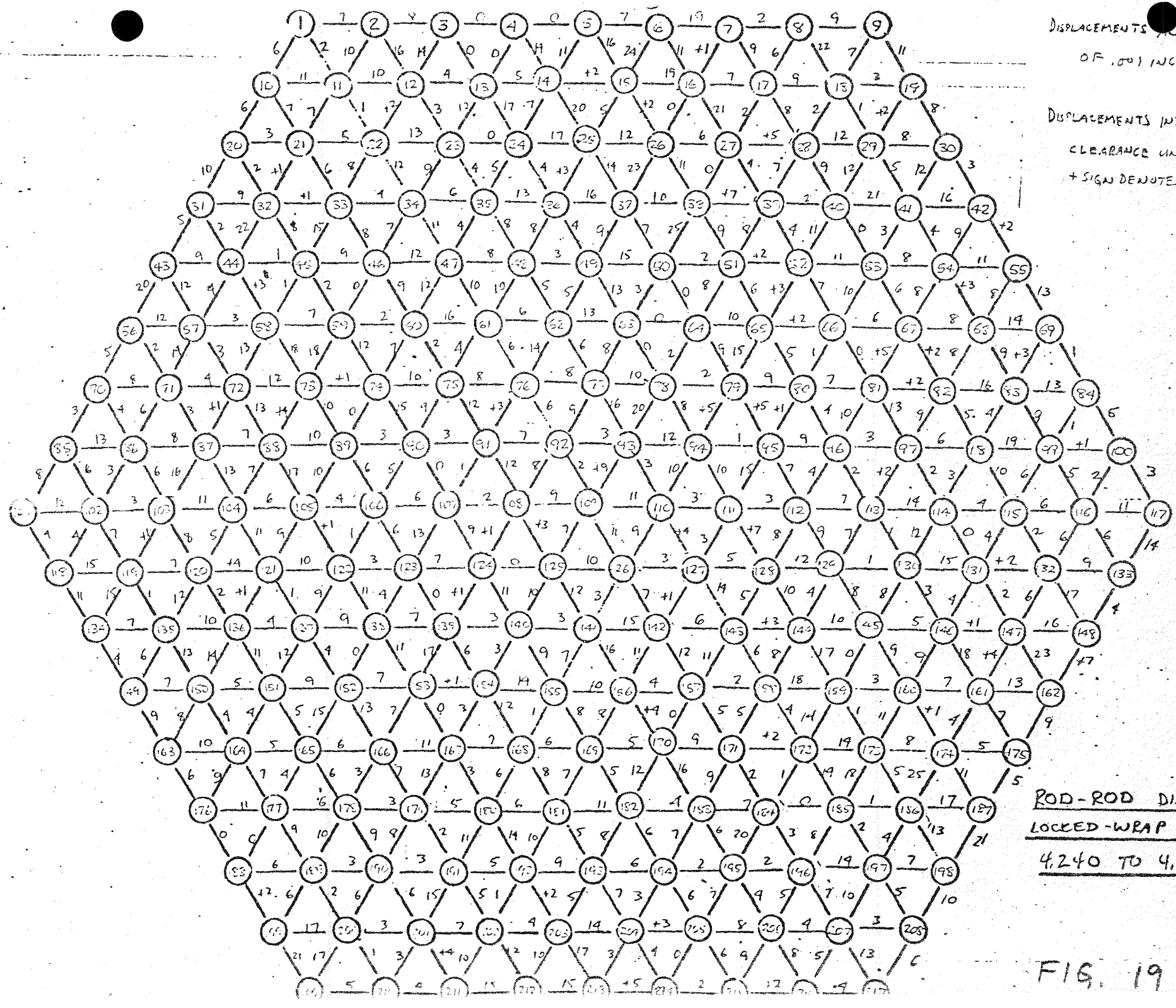

DISPLACEMENTS ARE IN UNITS OF .001 INCH (.0254 MM.

DISPLACEMENTS INDICATE DECREA. CLEARANCE UNLESS + SIGN

+ SIGN DENOTES INCREASE.

ROD-ROD DISPLACEMEN

LOCKED-WRAP BUNDLE

4.240 TO 4.140 A/F

FIG. 19

staggered start, and the locked wrap, respectively, with the units on the diagram representing increments of .001 inches (.0254 mm). Figures 16, 17 and 18 are for approximately .070 inch (1.78 mm) across-flats interference which has been applied to the nominal tight bundle. Figure 19 is for an additional .100 inch (2.54 mm) across-flats interference which has been applied to a bundle with an initial across-flats interference of .030 inch (.76 mm). Thus to quantitatively compare Figure 19 with Figures 16, 17 and 18, the displacements on Figure 19 should be decreased to 70% of the values shown.

The rod-to-rod displacement comparisons show that the softened bundles distribute the bundle compression displacements in a more uniform manner across the bundle. This is due to the nesting mechanism. Much of the straight start overall bundle compression displacement occurs in the region more immediate to the locations where the bundle edge wires contact the channel. Also several gross displacement patterns can be detected where a row-to-row relative motion is observed. These straight start bundle displacements are considered to be consistent with postulated dispersion mechanisms of Reference 3, which defines the dispersion mechanism of the straight start bundle to be the result of mechanically unstable load paths associated with punch planes, and that the pinch plane loads are a maximum near the bundle-to-channel contact region causing greater dispersion displacement at these locations. The nesting mechanism of the wireless bundle and the manner in which the mechanism is distributed across the bundle can be observed in Figure 17 and is particularly apparent when consideration is given to the manner in which the pinch plane is disrupted at the level of the optical targets in the rods. In the following sketches for the optical target level of the bundles the wires are at the plane where the wire spacer contacts the channel at the 10 o'clock flat. The wires are thus midway between

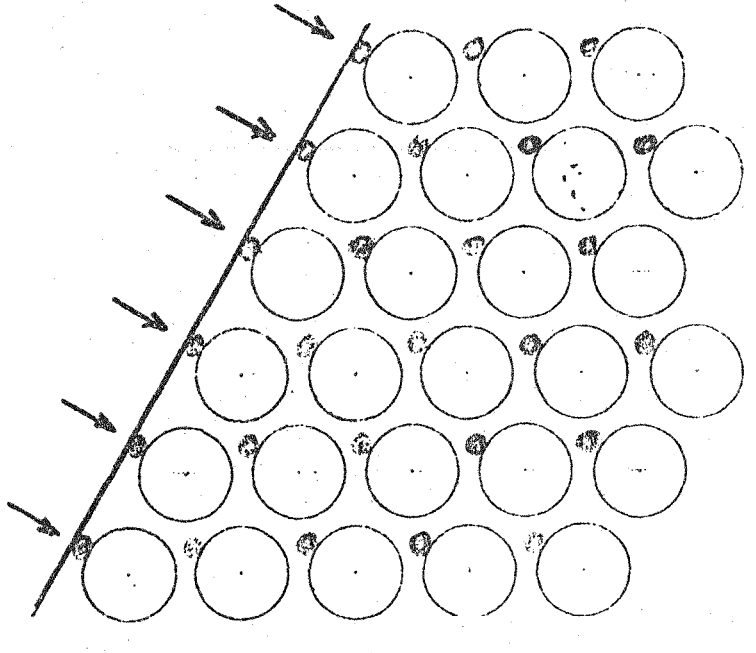

0°-0°-0°

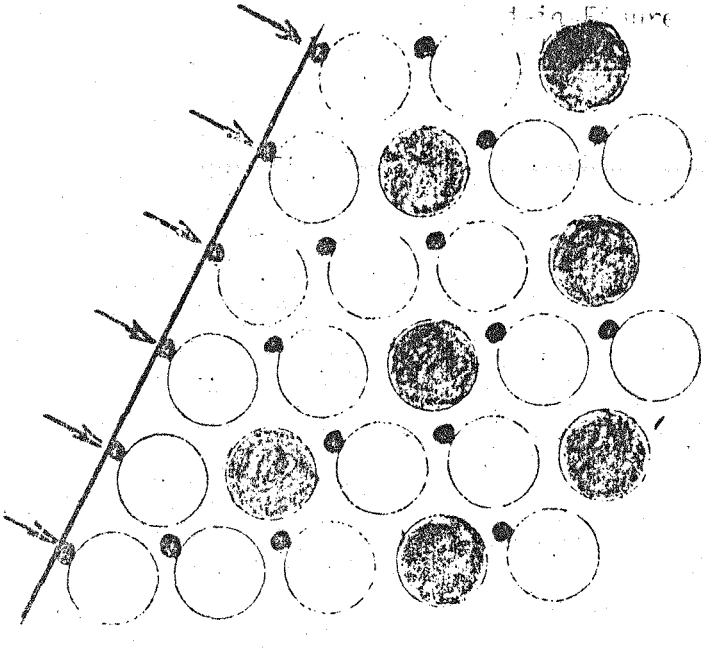

0°-0°-0° with wireless rods

two pinch planes, one pinch plane lying 1 inch (25.4 mm) above and the other 1 inch (25.4 mm) below. Thus, at the optical target level, groups of three rods can deflect toward each other, the groups being characterized by a wireless rod and the two rods at 9 and 11 o'clock with respect to the wireless rod. In Figure 17, the rods numbered 47,60 and 61 are a typical example of three such rods.

Figures 20 and 21 are additional vector plot and rod-to-rod displacement results for the wireless bundle, for a bundle across-flats compression of .155 inches (3.94 mm). In comparing Figures 12 and 20, it should be considered that different vector scales are used, with the basis for a scale being to consider the normal components to the 10 o'clock flat as being one-half of the across-flats compression. In comparing the rod-to-rod displacements between Figures 17 and 21, those of Figure 21 should be approximately 2.3 times as great as those of Figure 17 for linear behavior. The fact that those of Figure 21 are, in general, smaller than the expected increase is partially attributed to the errors in readings (which are compounded by taking small differences of large values) being independent of magnitude, and that a limited but random amount of displacement is associated with compaction and shifting due to "imperfections" such as tolerance, run-out on wires and rods, etc.

At the maximum compression of the wireless bundle, at various irregularly located places along the outer periphery of rods, several locations were observed where edge rod to edge rod spacing was decreased to minimal values of approximately .010 to .015 inches (.25 to .038 mm), as measured using a feeler gage. Numerous assorted gap sizes were seen elsewhere. At the optical target elevation no clearances as small as .010 inches (.25 mm) were observed, as indicated in Figure 21. (The .049 inch (1.24 mm) closure between rods 10 and 20, as identified in Figure 21, could not be observed because of the presence of the load pad.) At some locations the large closures of clearance will be attributed to the proximity of wireless rods in the adjacent interior row, however some large closures were observed which were not immediately adjacent to a wireless rod.

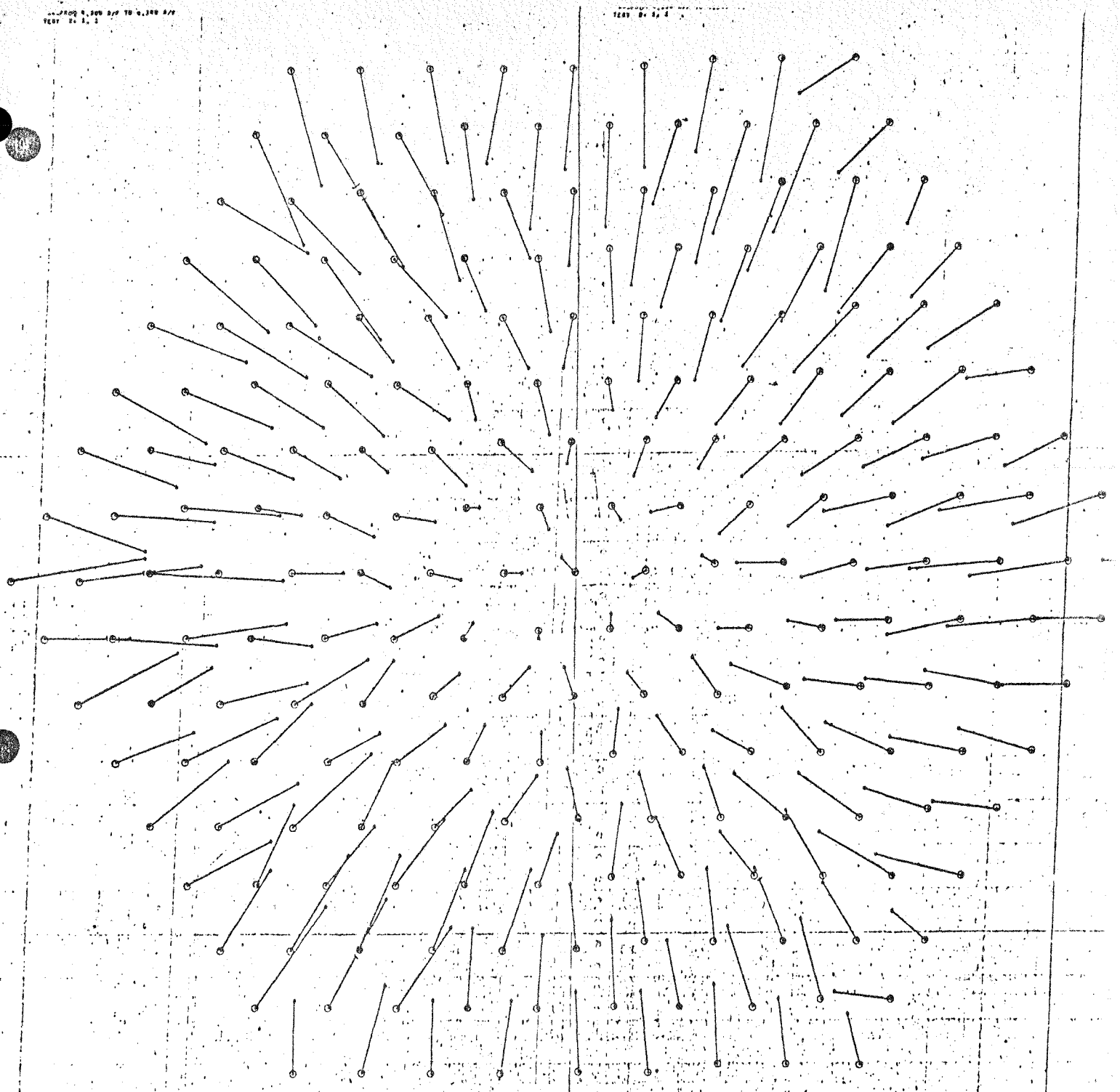

⊕ is the origin of displacement vector.
* is terminus of displacement vector.

Vector scale and rod original position scale differ by an order of magnitude.

0°-0°-0° WITH WIRELESS RODS

4.300 TO 4.140 A/F

FIG. 20

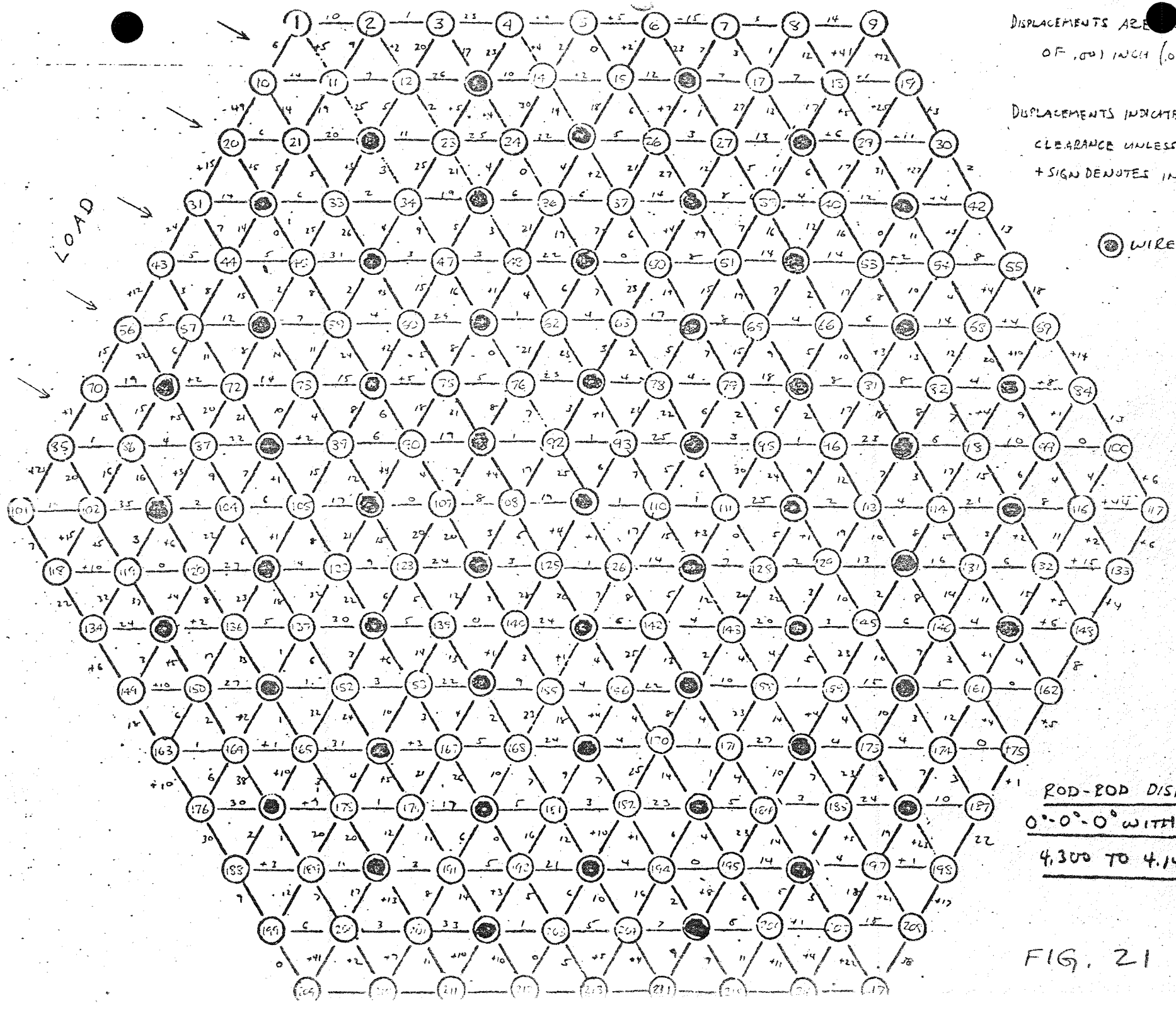

DISPLACEMENTS ARE IN UNITS OF .001 INCH (.0254MM.)

DISPLACEMENTS INDICATE DECREASED CLEARANCE UNLESS + SIGN. + SIGN DENOTES INCREASE.

WIRELESS

ROD-ROD DISPLACEMENT
0°-0°-0° WITH WIRELESS
4,300 TO 4.140 A/F

FIG. 21

Large variation of edge rod spacing was not as readily observed with the straight start bundle because of the limited degree of bundle compression to which it was subjected. However, scaling the closure between rods 31 and 43 of Figure 16 by the bundle compression relative across-flats displacement yields a comparable closure.

The staggered start bundles displayed small rod-to-rod clearances at the edge rods, irregularly located throughout the bundle. The minimum observed were approximately .005 inches (.13 mm) greater clearances than were observed during testing of the wireless bundle, which preceded testing of the staggered start bundles.

Figure 22 is a photograph taken of the wireless bundle at maximum compression. A nonuniformity of the displacements results in the shadow variation is readily observed along the left half. The axial mid-point between load pads is located by isometrically traversing from the hole in the metal strip to the bundle. The variation shown, which was typical at all faces of the wireless bundle, occurred in other bundle configurations also, but not to the extent as in the wireless.

Figures 23 and 24 are additional vector plot and rod-to-rod displacement results for the locked wrap bundle for a bundle across-flats compression of .180 inches (4.57 mm). These exhibit a continuation of the behavior observed for the lesser degree of compression, .100 inches (2.54 mm).

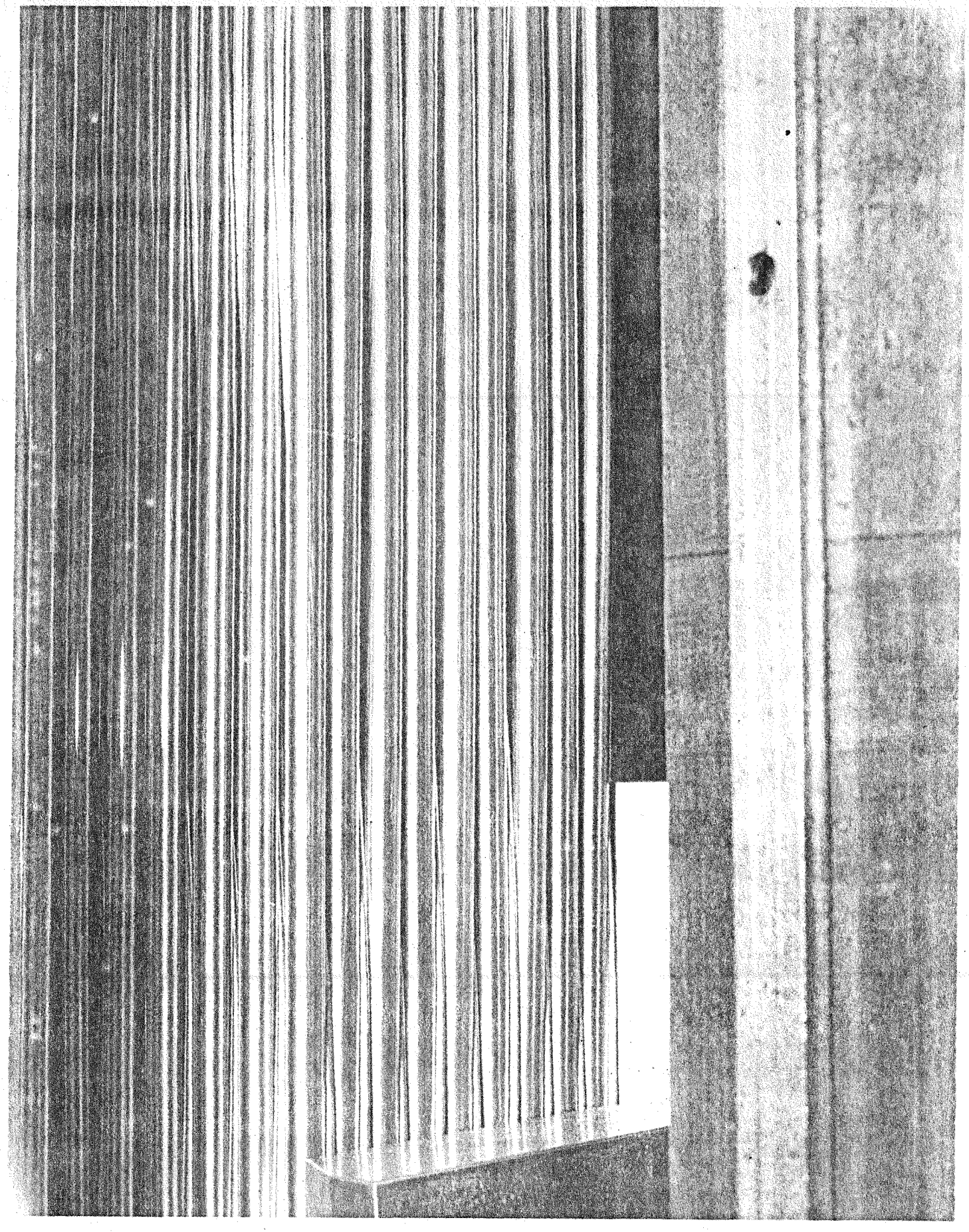

Figure 22 Wireless Bundle at .160 Inch Across-Flats Compression

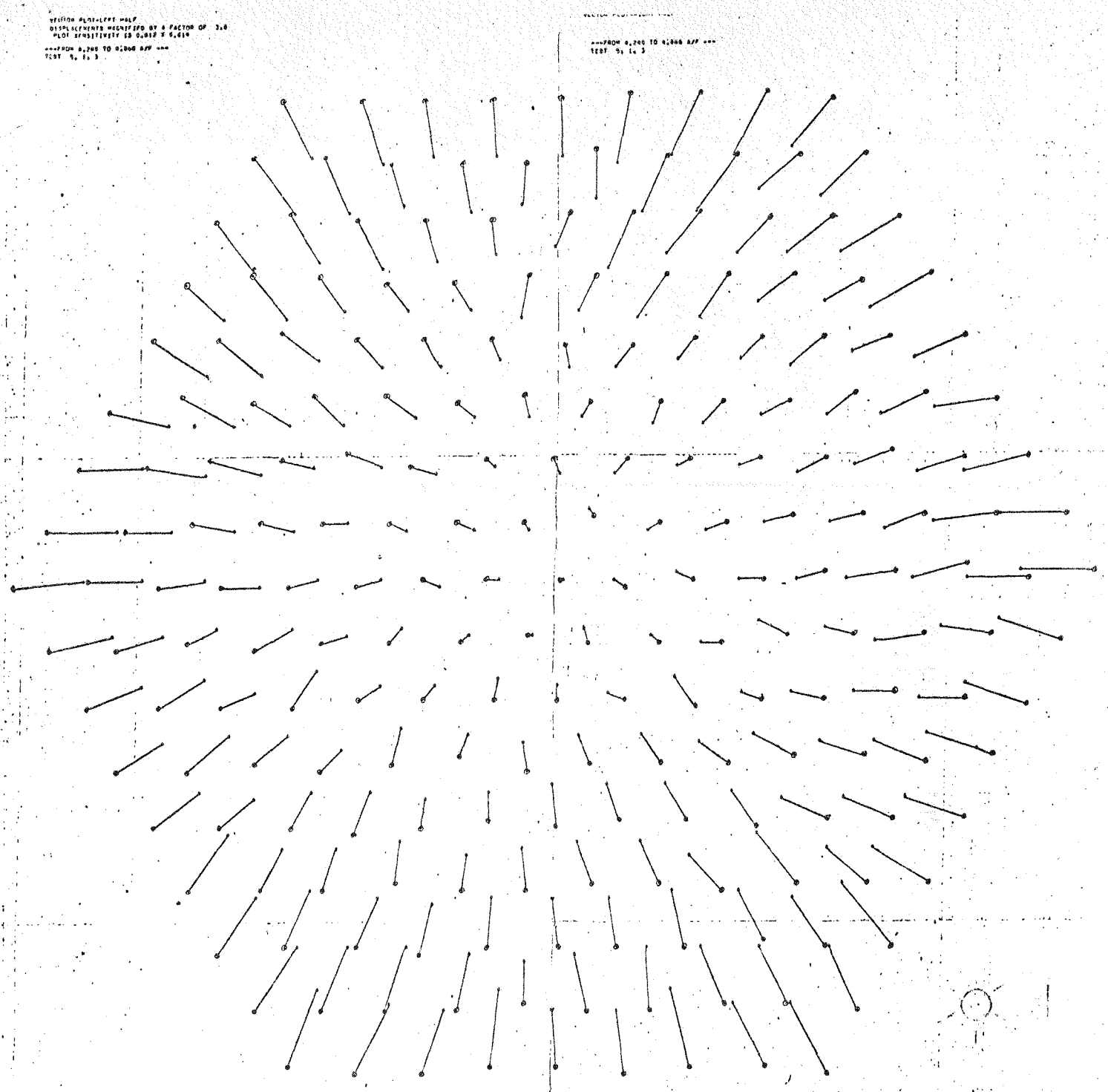

⊕ is the origin of displacement vector.
* is terminus of displacement vector.

Vector scale and rod original position scale differ by an order of magnitude.

LOCKED WRAP ROD DISPLACEMENTS
4.240 TO 4.060 A/F

FIG. 23

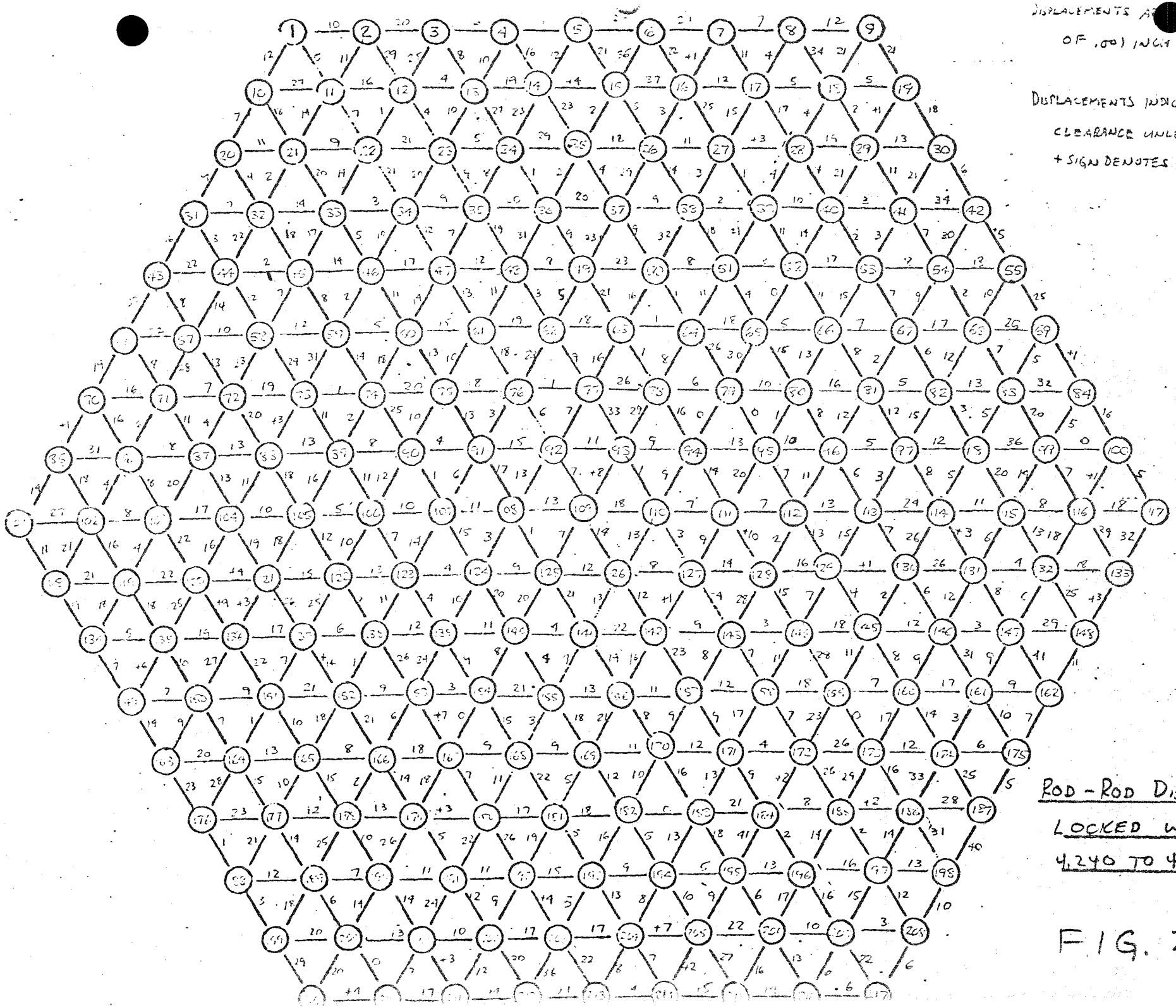

DISPLACEMENTS ARE IN UNITS OF .001 INCH (.0254 MM.)

DISPLACEMENTS INDICATE DECREASE CLEARANCE UNLESS + SIGN. + SIGN DENOTES INCREASE.

ROD - ROD DISPLACEMENT

LOCKED WRAP

4.240 TO 4.060 A/F

FIG. 24

7.0 LOCKED WRAP BUNDLE EXPERIENCE

In Sections 5 and 6, a discussion of the compression test results was presented for the five bundle configurations tested. From the evaluation of the data it appears that the static mechanical behavior of the locked wrap bundle is superior to the others tested in terms of providing displacements associated with optimum fuel rod bundle in-reactor performance. Experience with the assembling, handling, and personal observation of the design indicates the necessity of a continued development program to prove the locked wrap a viable design.

During the procedure of loading the locked wrap bundle into the compression testing fixture, handling problems arose which necessitated modifying the final steps of the loading procedure. The occurrence of rod-to-rod clearances of the order of a wire diameter within the bundle during handling could disturb the locked configuration. It has been described in Section 4 that the manner in which three wires engage each other, tends to lock the rods together at each of the wire cluster locations. As one of the three clustered wires tries to escape the locked position, a section of that wire immediately above or below the locked plane is blocked by the wire of one of the other two rods which pass through the same rod-to-rod clearance flow channel. Thus to insure that locked wires do not escape, the bundle should be assembled and handled such that excessive clearances (of the order of a wire diameter) do not develop and allow wires to escape the clusters. It is not to be inferred that temporary clearances will result in wires escaping the clusters, but only that the locked wires cannot escape unless the clearances occur. Clearances which could have allowed locked wires to escape may have occurred during the loading of the test bundle, although no evidence of this was observed.

A special handling fixture was fabricated to assist in assembling the locked-wrap bundle, transporting it to the test fixture, and loading it into the fixture. Associated procedures were also specified. Preliminary to assembling the 217-rod test bundle, a 169-rod trial bundle was assembled and loaded into the compression test fixture. The 169-rod bundle was assembled from the rods previously used for the other four test bundles, following the completion of the tests on these bundles. These rods were used so as to minimize the possibility of damage to the test bundle rods. As the trial bundle rods are .056 inch (1.42 mm)

diameter wire and the test bundle rods use .0465 inch (1.18 mm) diameter wire to obtain the same rod-to-rod spacing, the trial bundle was limited to 169 rods to allow it to be loaded into the test fixture. The same handling fixture was used for both the 169 and 217 rod bundles by affixing shims to account for the slight across flats dimension differences.

Figure 25 shows the bundle partially assembled in the rigid handling fixture. (The 0°-120°-240° staggered starts can be seen on the exposed rod layer.) It was determined through experience that the handling fixture was required to have a slight across-flats interference to keep the extremely soft bundle from flattening due to the nesting mechanism which provides the bundle compression compliance. Although the bundle weight is not high with the hollow rods, it must be recognized that the bundle can be extremely soft for a one-directional load as compared to the multi-axial loading during compression in the test fixture. It was also thought that the bundle would be more stable during handling if it were compressed.

Figure 26 shows the fully assembled bundle in the future, looking at the top end. At the top of each rod is placed a rubber o-ring of 1/16 inch (1.58 mm) thickness. The o-rings are slightly staggered across the bundle so as not to contact each other. To the right of the bundle is a combination lifting device as well as a centering device for when the bundle is in the test fixture. The rubber o-rings provide a compliant rod-to-rod and rod-to-lifting device spacer as well as providing high friction for axial load shear transfer across the bundle. Figure 27 shows the lifting device in place and the bundle ready to be transferred by crane to the compression test fixture. Figure 28 shows the test bundle being lowered into the compression test fixture. The handling fixture, which is disassemblicable, has just had a second section removed, and the exposed section of the bundle is about to be lowered into the test fixture.

At this time it is useful to consider the procedure being followed as the bundle is lowered into the test fixture. The individual load pads in the test fixture have all been aligned and form a hexagonal "chamber" whose across flats dimension is 4.400 inches (111.76 mm). The chamber walls consist of

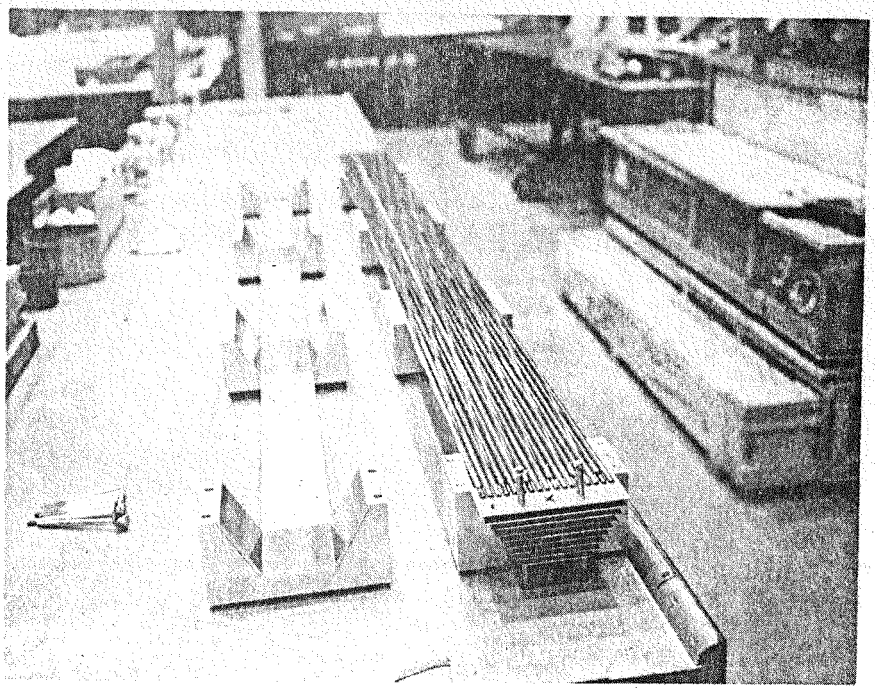

FIGURE 25
PARTIALLY ASSEMBLED LOCKED WRAP BUNDLE

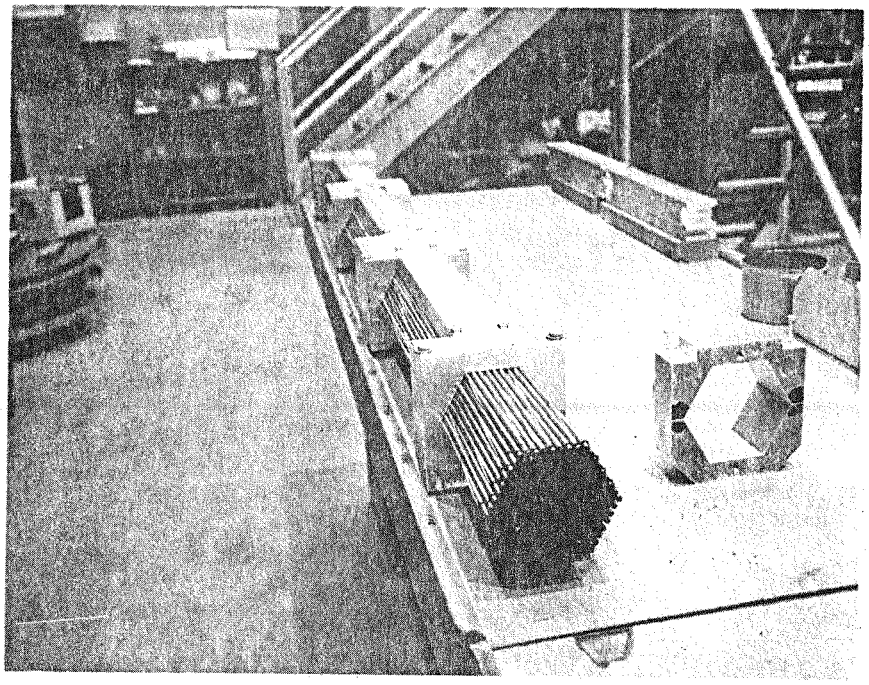

FIGURE 26
FULLY ASSEMBLED LOCKED WRAP BUNDLE

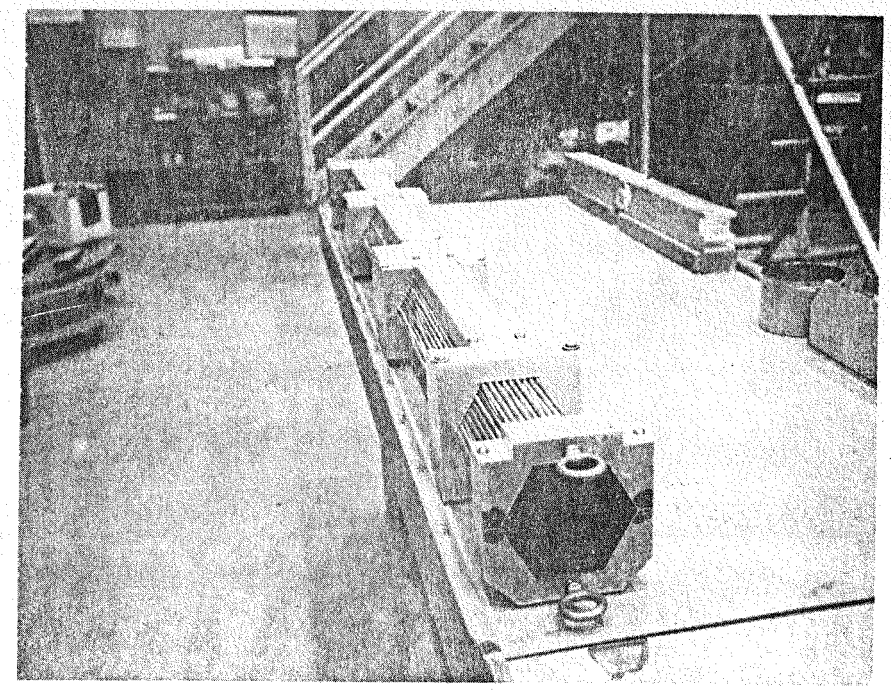

FIGURE 27
LOCKED WRAP BUNDLE READY FOR TRANSPORTING

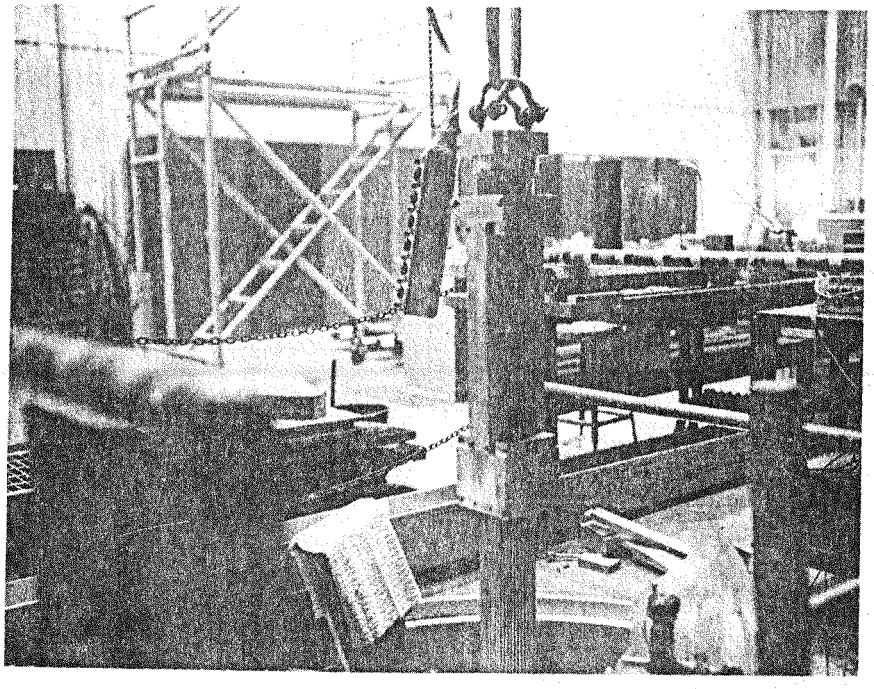

FIGURE 28
LOCKED WRAP BUNDLE BEING LOADED INTO TEST FIXTURE

alternate load pads of 3-inch (76.20 mm) and 6-inch (152.40 mm) lengths with a 1.5-inch (38.10 mm) opening between the pads. This near continuous coverage of the bundle by the load pads is necessary because of the extreme staggering of the wire wraps. Although the test bundle across-flats dimension (outer wire surface to outer wire surface) is 4.270 inches (108.46 mm), the 4.400-inch (111.76 mm) across-flats spacing is needed to allow ample clearance for the rod support rails and the rail locking pins (which can be seen in Figure 25). As the bundle is slowly lowered into the test fixture the rails and locking pins are manually guided past the load pads. As the upper load pads are cleared by the rails they are then moved inward to a corresponding across-flats dimension of 4.280 inches (108.71 mm), providing a simulated bundle to channel clearance of .010 inches (.25 mm). The procedure was implemented to minimize the chance of large rod to rod clearances occurring, which could potentially lead to unlocking of the locked wires.

With the bundle in place the load pads were moved to the tight bundle across-flats dimension of 4.270 inches (108.46 mm). At this time the bundle was examined by manual manipulation of the exposed edge rods. A loose feeling of the edge rods was observed. In an effort to assess this further observation, compression of the bundle was initiated prior to the procedure of taking the optical measurements. The bundle compression spring constant exhibited during this loading was approximately two-thirds of that anticipated from the pretest predictions, the pretest prediction being an extrapolation to a 217-rod bundle of NASTRAN computer code results for a 37-rod bundle. It was observed that with 0.030-inch (6.75 mm) across-flats compression the edge rods continued to feel loose in response to manual manipulation in the lateral direction. At approximately 0.100 inch (2.54 mm) across-flats compression, the looseness observed earlier no longer existed.

A possible explanation for the lower spring constant and the relative looseness of the edge rods is postulated and can be explained using the schematic representation of Figure 3. Figure 3 shows that two types of edge row rod supports

occur, one type occurring along the 2,6, and 10 o'clock flats and the other along the 12,4 and 8 o'clock flats. At the 2,6, and 10 o'clock flats, the edge wire which spaces the bundle from the channel is normally part of a triple point cluster, but the cluster is incomplete due to its being at an edge row. At the 12, 4, and 8 o'clock flats the triple point cluster is also incomplete but the bundle-channel clearance is provided at a wire position which is axially midway between triple point axial positions. At the 12, 4, and 8 o'clock flats, the lateral support provided by the two contacting wires is not fully effective because of not being locked by the third wire. The resulting two wire contact is relatively unstable and slight relative movement of the wires could be observed when these rods were normally displaced laterally. At the 2,6, and 10 o'clock flats, the friction between the wire contact and the loading pad apparently provides negligible lateral support compared to a triple point cluster, and hence the lateral looseness at these rods.

Figure 29 is the bundle compression data for the three tests in which the bundle was subjected to a high degree of compression. The maximum compression was limited by the bridging of the loading pads. After the bridging was detected (by a sudden hard contact at a location away from the six load cell locations), close inspection of the load pads showed that pad-to-pad contact had been made at many bundle locations, including several at the load cell locations, but were at pad corners and were due to very slight cocking or rotating of the pads. Upon manually adjusting the rotation to eliminate the slight bridging, the "apparent" bundle compression decreased to the value indicated on Figure 29.

Because of the loose feel of the bundle at low compression and the bundle softness throughout its compression, it was decided to record optical data at the subsequent unloading and to compare these data with the original optical data. For a fully elastic bundle, which is expected of the locked-wrap bundle because of its complete rod-to-rod nesting capability, the rods would return to initial positions (except for displacement components associated with imperfections).

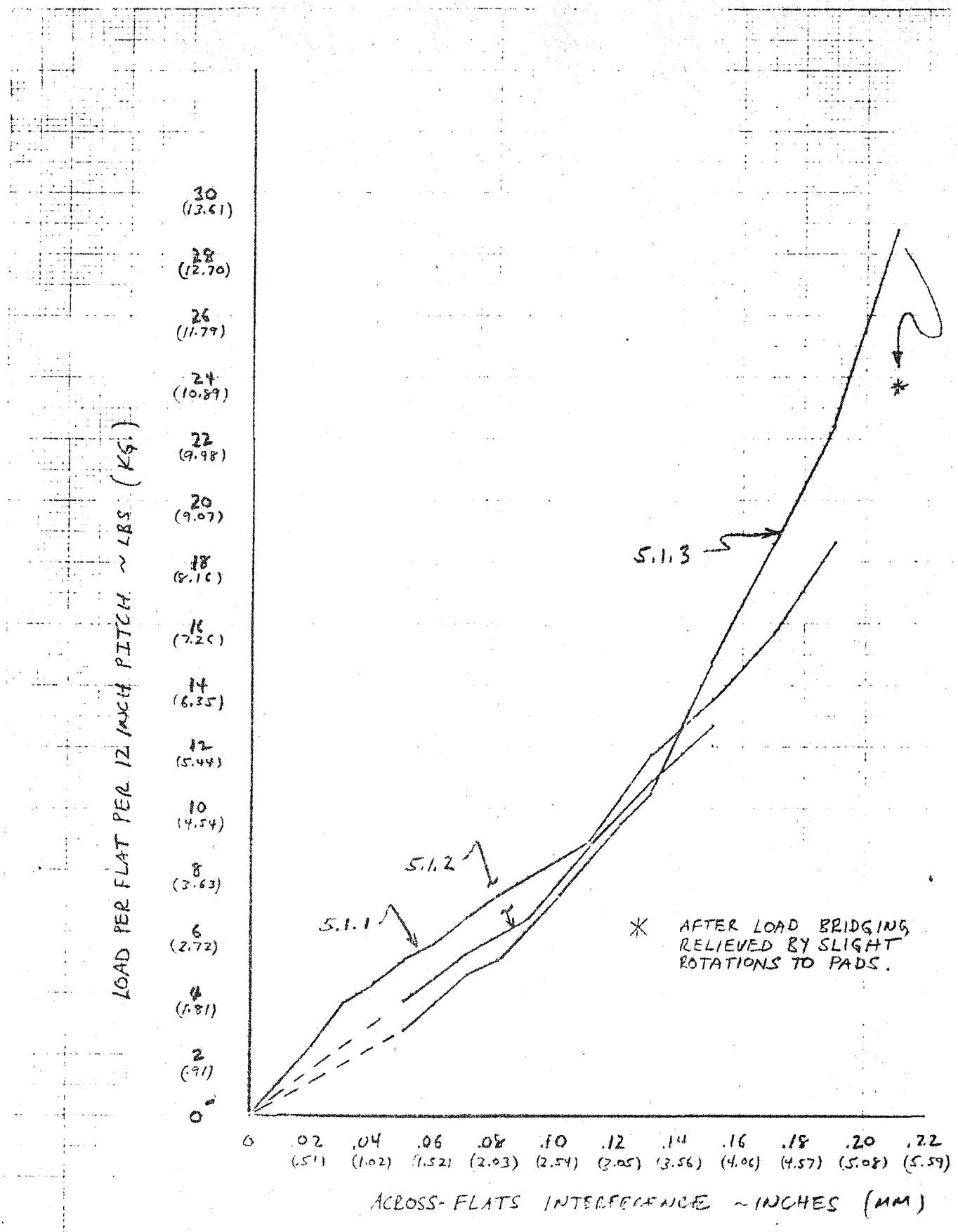

LOCKED-WRAP COMPRESSION DATA

FIG. 29

The initial loading and the final unloading data were taken at 4.240 inches (107.70 mm) across-flats dimension, which represents a 0.030-inch (0.76 mm) across-flats bundle compression from the tight bundle dimension. The maximum across-flats bundle compression was 0.180 inches (4.57 mm) greater than that at the initial data compression. The difference between the initial loading and final unloading position coordinates of the rods, calculated as a standard deviation so as not to average positive and negative differences, was approximately 3.5 mils (0.09 mm). The variation in individual rod differences was randomly distributed throughout the bundle. As these differences are considered small, it is concluded that the bundle recovery at unloading was fully elastic. (Due to the extreme bundle softness, at the latter stage of unloading it was necessary to manually assist moving the load pads after relieving the loading screw. However, this in no manner should have affected the rod displacements.)

8.0 FUEL ROD BURNUP LIMITS FOR ADVANCED DESIGNS

LMFBR fuel rod burnup limits are dependent on the complex interaction of several mechanisms. It is convenient to investigate the burnup limit by the following assembly parameters:

1. Channel-to-Channel Contact

   Irradiation-induced swelling and creep in the presence of the channel wall differential pressure cause the channels to dilate and eventually touch. For the CRBR fuel assembly design, adjacent channels are separated by two load pad thicknesses of 0.085-inch (2.16 mm) or 0.170-inch (4.32 mm) total.

2. Interior Rod Closure

   A previous study has shown that when two interior rods approach within 12-15 mils (0.3-0.4 mm) of each other the probability of cladding failure is increased significantly ($\approx$ 15%) due to the hot spot which occurs. 12-15 mils rod-to-rod spacing represents a threshold below which sealed plenum fuel rod performance is seriously degraded.

3. Edge-Rod-to-Channel Contact

   Another threshold limit for fuel rod performance is set by the contact of an edge or corner rod with the channel.

Various wire-wrap assembly designs can be compared in terms of these limits and the resulting maximum fuel burnup. A truly advanced design would be one permitting the achievement of the CRBR target burnup goal of 150,000 MWD/Te (approximately 25 x 10^{22} n/cm^2 fluence). For this study, CRBR assembly design values are used, including 34 mils (.86 mm) clearance between the rod bundle and the channel at beginning-of-life (provided to allow easy assembly). Table 2 presents the core parameters and temperatures used in the study. The material properties are those of reference 4.

Figure 30 is a plot of the observed maximum bundle-channel gap reduction with across-flats interference, taken directly from the Phase I test data. The across-flats interference is the differential bundle-to-channel growth after

Table 2

CRBR CORE PARAMETERS

Peak Axial Fast Fluence	2.5×10^{23}
Peak Axial Fast Flux	3.5×10^{15} n/cm^2-sec
End of Life Time	20,000 hr (est.)
ΔP Across Channel Wall-bot	38 psi
- core top	25 psi
Temperatures Channel Bottom	722°F
Channel Top	965°F
Core Length	36"
Channel Wall Thickness	.120"
Channel Across Flats Width	4.335"
Bundle-Channel Assembly Gap	.034"
Material	20% CW 316 SS

CRBR BUNDLE AND CHANNEL TEMPERATURES

Axial Location	Channel Temperature	Bundle Temperature
0	722°F	783°F
6	752°F	840°F
12	790°F	917°F
18	835°F	992°F
24	883°F	1060°F
30	927°F	1112°F
36	965°F	1148°F

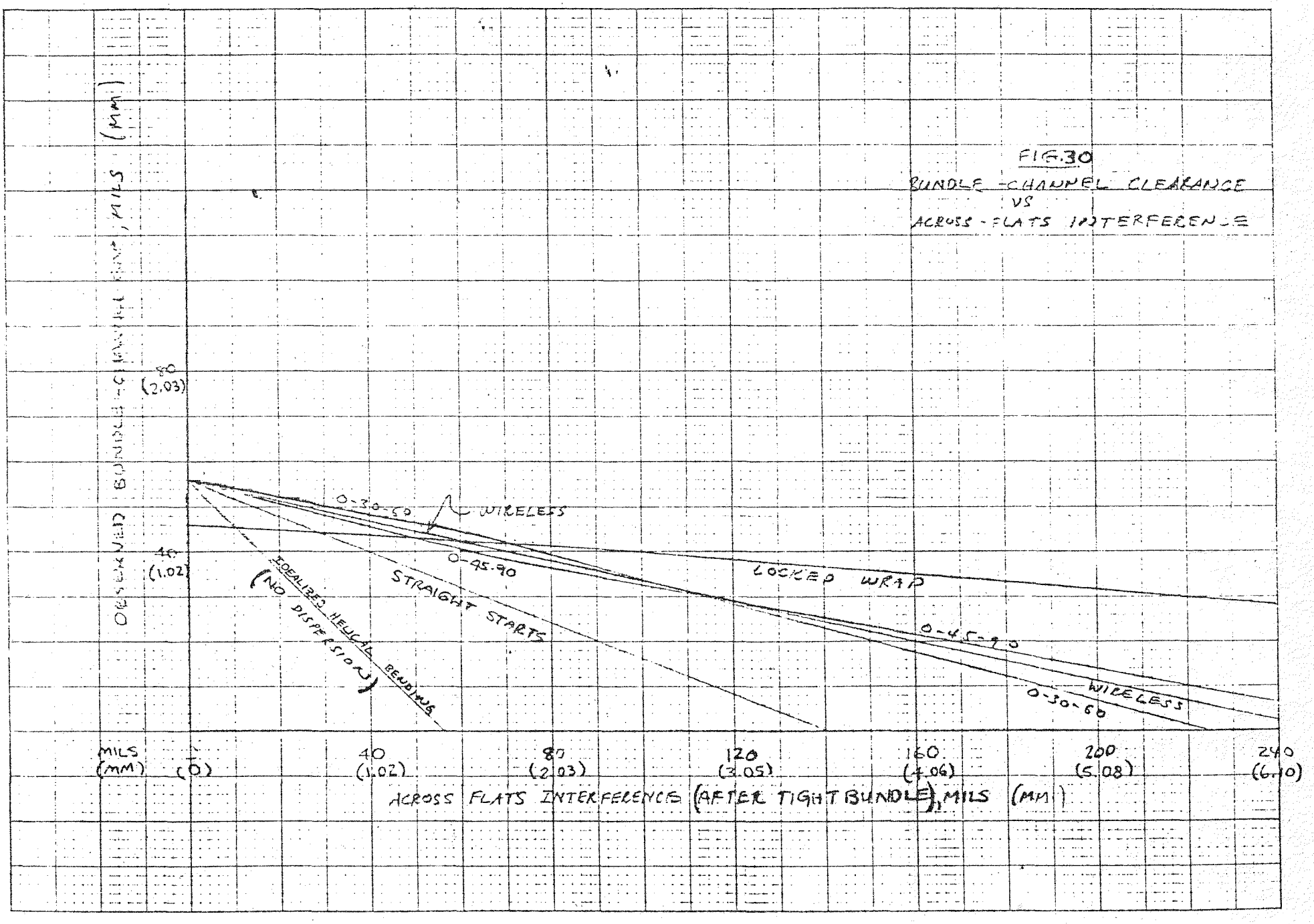
FIG. 30
BUNDLE - CHANNEL CLEARANCE
VS
ACROSS - FLATS INTERFERENCE
OBSERVED BUNDLE - CHANNEL CLEARANCE, MILS (MM)
80 (2.03)
40 (1.02)
0-30-60 WIRELESS
0-45-90
STRAIGHT STARTS
(EQUALIZED HEIGHT REMOVED)
LOCKED WRAP
0-45-90
WIRELESS
0-30-60
MILS (MM)
0
40 (1.02)
80 (2.03)
120 (3.05)
160 (4.06)
200 (5.08)
240 (6.10)
ACROSS FLATS INTERFERENCE (AFTER TIGHT BUNDLE), MILS (MM)

the 34-mil (.88 mm) assembly clearance has closed. If dispersion or rod-to-rod nesting did not occur, the .056-inch (1.42 mm) gap (i.e., wire diameter) would have closed at an across-flats interference of .056 inch (1.42 mm) because of the bundle helical bending without relative rod-to-rod displacements. The curves were extrapolated to determine the limiting interference, that is, where the minimum bundle-channel gap becomes zero. The locked wire wrap exhibits the best clearance behavior of all the bundle configurations tested.

Similarly, Figure 31 is a plot of maximum interior rod-to-rod gap reduction with cross-flats interference, taken from the test data. Had there been no dispersion, the rod-to-rod spacing would not have changed for the straight start bundle. The interference corresponding to a minimum residual gap of 15 mils (.4 mm) for each design is indicated. The large increase in allowable interference between the locked wrap bundle and the reference straight-start bundle is significant. It should also be noted that these two plots are quite conservative as the absolute minimum gaps have been plotted, rather than attempting any statistical evaluation of the data.

The five designs were first compared using the CRBR structural material, 20% cold-worked Type 316 stainless steel for both cladding and channel. Results for the reference straight-start bundle are presented in Figure 32. The axial distributions of cross-flat interference are shown for four cases: (1) the target end-of-life fluence (25×10^{22} n/cm^2), (2) the interior rod-to-rod limit (conservatively chosen as being 15 mils or .4 mm), (3) the edge-rod-to-channel limit (the point at which the fuel rod touches the channel), and (4) the channel-to-channel contact limit. The limiting constraint on this basis is seen to be the 15-mil rod-to-rod minimum allowable gap which occurs at 18.5×10^{22} n/cm^2 fluence or 110,000 MWD/Te burnup. This is somewhat less than the channel-to-channel contact limit, 20.5×10^{22} n/cm^2.

When the advanced designs are employed, the bundle interference limits are extended and channel-to-channel contact is limiting in every case. Thus, all the advanced designs for 20% CW Type 316 stainless steel are predicted to reach fluences of 20.5×10^{22} n/cm^2, 10% greater than the reference design, but still 18% less than the CRBR target goal.

FIG. 31

ROD - ROD CLEARANCE
VS
ACROSS - FLATS INTERFERENCE

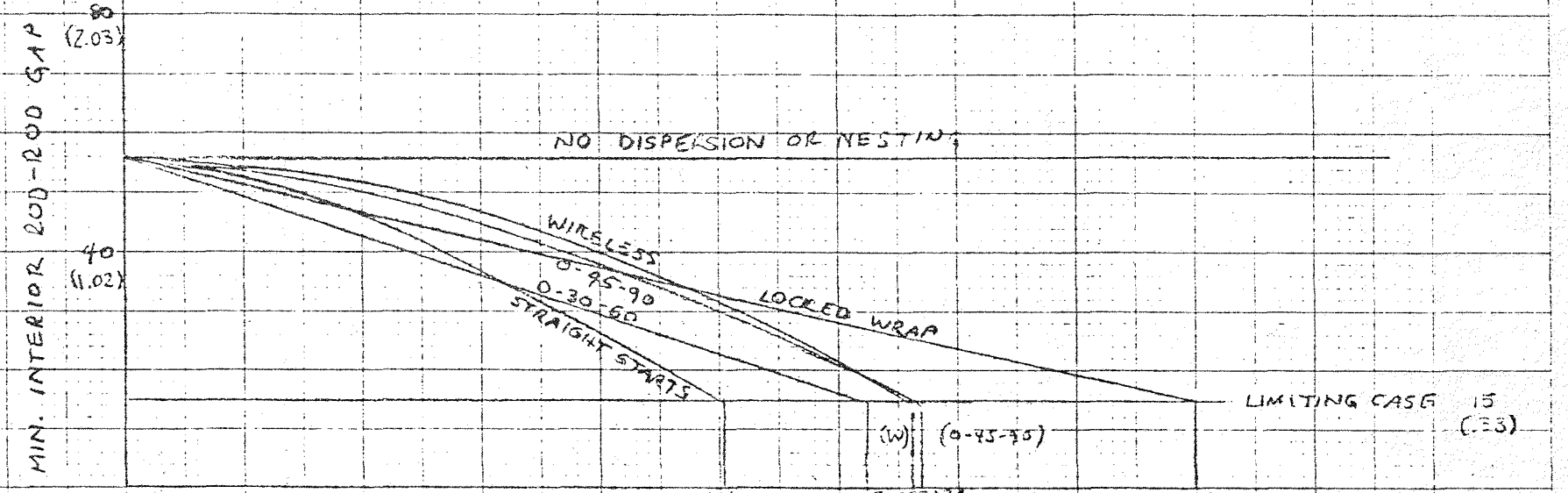

FIG. 32

STRAIGHT STARTS INTERFERENCES WITH 20% C.W. TYPE 316 S.S. CHANNEL AND CLADDING

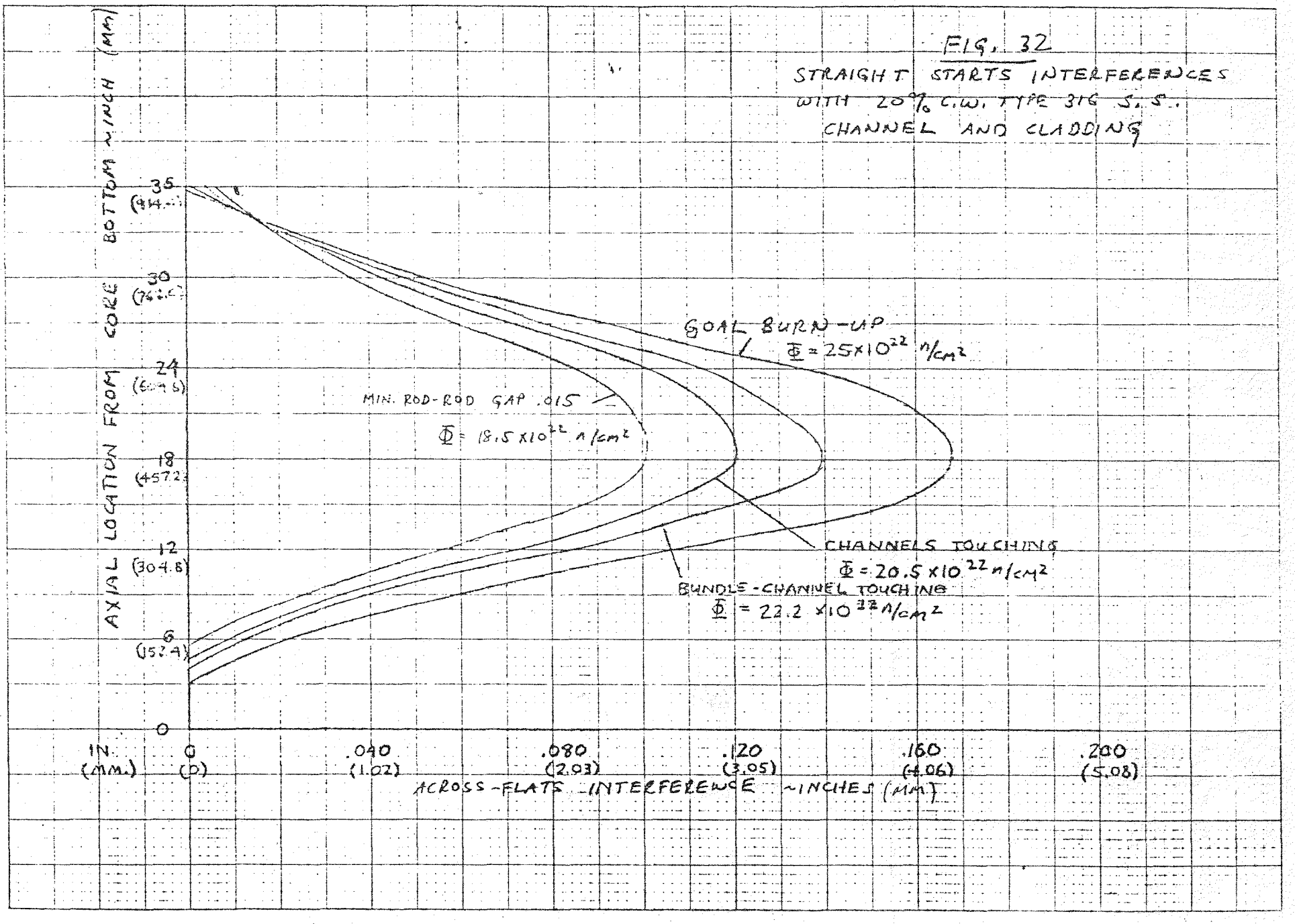

Since the critical limit with stainless steel channels is channel-to-channel contact, the use of PE-16 (with its relatively low swelling and creep) for the channel material was investigated. Calculations show that the use of PE-16 extends the channel-to-channel contact limit well beyond the target fluence of 25 x 10^{22} n/cm^2. It should be noted that, in addition, many core restraint system problems are alleviated by a low swelling channel material.

However, the use of a PE-16 channel and cold-worked 316 SS cladding does increase the problems of bundle-channel interference. For the reference, straight-start design, the limiting constraint (considered here to be a 15 mil or .4 mm minimum rod-to-rod gap) now occurs at 16.9x10^{22} n/cm^2, 8.6% lower fluence than when a cold-worked 316 SS channel is used. Similarly, the edge-rod-to-channel closure limit is also reached sooner.

The effect of using the various advanced designs is summarized in Table 3. When PE-16 is used as the channel material, the limiting constraint for each design is the minimum allowable gap between interior rods. This limit occurs with PE-16 at fluences slightly lower than when 20% CW 316 stainless steel channels are used. For example, the wireless bundle now reaches 19.7x10^{22} n/cm^2 fluence and 118,000 MWD/Te burnup and the 0-45-90 staggered-start bundle achieves 19.8x10^{22} n/cm^2 fluence and 118,000 MWD/Te. These designs show approximately an 8% burnup gain over the current reference (with 316 SS channel) but fall short of the target goal of 150,000 MWD/Te.

Additional area to accommodate bundle-channel interference may be provided by channel ballooning. That is, in addition to dilating, the channel distorts into a more circular form. Table 4 shows that approximately 7000 MWD/Te additional burnup is possible with each design if this entire area is effective in accommodating interference. (This will be experimentally determined in the Phase II tests to be conducted later this fiscal year.)

The best design, in terms of achievable fuel lifetimes, is clearly the locked wrap. This design reaches 142,000 MWD/Te, 95% of the target goal. When credit is taken for channel ballooning, the locked-wrap design achieves 152,000 MWD/Te burnup. Thus, the locked wrap is truly an advanced design worth further development.

TABLE 3

Burnup Comparison of Designs

Design	Channel* Material	Critical Limit	Max.** Fluence (n/cm^2)	Max.** Burnup (MWD/Te)
Straight Starts	20% CW 316 SS	Int. Rod-Rod	18.5×10^{22}	110,000
0-30-60	20% CW 316 SS	Channels touch	20.5×10^{22}	122,000
0-45-90	20% CW 316 SS	Channels touch	20.5×10^{22}	122,000
Wireless	20% CW 316 SS	Channels touch	20.5×10^{22}	122,000
Locked Wrap	20% CW 316 SS	Channels touch	20.5×10^{22}	122,000
Straight Starts	PE-16	Int. Rod-Rod	16.9×10^{22}	101,000
0-30-60	PE-16	Int. Rod-Rod	19.0×10^{22}	114,000
0-45-90	PE-16	Int. Rod-Rod	19.8×10^{22}	119,000
Wireless	PE-16	Int. Rod-Rod	19.7×10^{22}	118,000
Locked Wrap	PE-16	Int. Rod-Rod	23.7×10^{22}	142,000

TABLE 4

Burnup Comparison of Designs

Assuming all additional space provided by ballooning of channel can be utilized to relieve interference.

Design	Channel* Material	Max. Fluence** (n/cm^2)	Max. Burnup** (MWD/Te)
Straight Starts	20% CW 316 SS	20.5×10^{22}	122,000
0-30-60	20% CW 316 SS	20.5×10^{22}	122,000
0-45-90	20% CW 316 SS	20.5×10^{22}	122,000
Wireless	20% CW 316 SS	20.5×10^{22}	122,000
Locked Wrap	20% CW 316 SS	20.5×10^{22}	122,000
Straight Starts	PE-16	18.0×10^{22}	108,000
0-30-60	PE-16	20.2×10^{22}	121,000
0-45-90	PE-16	21.0×10^{22}	126,000
Wireless	PE-16	20.9×10^{22}	125,000
Locked Wrap	PE-16	25.3×10^{22}	152,000

* All fuel rods are 20% CW Type 316 SS.

**Based on 150,000 MWD/Te at 25×10^{22} n/cm^2.

The following conclusions can be drawn from the analysis performed in this section:

(1) For the reference straight-start wire-wrap fuel assembly studies, the internal rod-to-rod gaps are predicted to be reduced to be equal to 15 mils prior to channel-to-channel touching, i.e., the primary burnup limit is rod-to-rod gap reduction.

(2) For 20% CW 316 SS fuel assemblies the use of any of the proposed advanced wire-wrap concepts would improve the bundle compression behavior such that channel-to-channel touching becomes the primary burnup limit.

(3) The use of a PE-16 channel in conjunction with 20% CW SS fuel rods minimizes channel ballooning at the expense of internal rod-to-rod gaps. In the case of the proposed advanced wire-wrap designs the locked-wrap concept with its low stiffness and uniform displacement behavior exhibits, by a significant margin, the best burnup capability (142,000 MWd/Te).

The above conclusions are based on the analysis of a typical CRBR fuel assembly. These results indicate that with near-term technology (a 20% CW SS locked-wrap fuel rod bundle with a P-16 channel) burnups approaching 150,000 MWd/Te are possible. This represents a 30% gain in burnup over the reference CRBR design. Additional gains in burnup may be possible for an optimized design where the channel-to-channel gap is traded off against channel wall thickness and the parameters of the fuel rod bundle.

9.0 RECOMMENDATIONS

Two advanced wire-wrap bundle designs are identified for further development; the wireless-rod-softened straight-start and the locked wrap designs. The wireless is thought of as near-term in that a minimal development program is required. The locked wrap is thought of as longer term or subsequent generation as a much more extensive development effort is required. Ultimately the superior design will depend considerably on further technological developments involving both core components behavior and overall plant operating economics. As examples, if a high degree of bundle-channel interaction must be accommodated, the locked wrap design potentially may be very superior; if lower fuel assembly pressure drop is the determining factor than the wireless bundle may be superior. (It is not known that the wireless bundle will have a lower pressure drop than the locked wrap, but the wireless bundle is predicted to have a lower pressure drop than the straight-start bundle.) The following recommendations are made for further development of these bundle designs.

Wireless

Plans to irradiate wireless bundles in FFTF should be considered. For immediate consideration a modification to standard FFTF bundles should be implemented by either using a maximum number of wireless rods (55) or a boot-strapping scheme which uses several combinations of wireless rods. It should be noted that one "wireless" bundle is currently undergoing irradiation in EBR-II (see Appendix).

Hydraulic testing of the wireless assembly should be considered to determine pressure drop characteristics and to examine the flow induced vibration effects. This may be particularly useful if coupled with a fabrication program directed at reducing the bundle assembly porosity.

Fabrication development, other than exclusion and inspection features to insure proper positioning of the distributed wireless rods, should address the possibility of utilizing the softer bundle compression characteristics to minimize the bundle clearance at assembly, decreasing fretting problems associated with bundle porosity.

Locked Wrap

Further development of the locked wire-wrap concept is required in the following areas

1) bundle assembly procedures

2) handling and shipping procedures

3) bundle hydraulic (including vibration performance).

The major concern for all the above development areas is that the much reduced stiffness (2 orders of magnitude as compared to straight start) of the locked-wrap bundle will lead to significantly different behavior. Satisfactory completion of the above development tasks should precede irradiation of experimental fuel assemblies.

REFERENCES

1. J.R. Punches, "Interim Justification Study for F11B," GR Document NEDG-19317, June 15, 1973.

2. R.B. Baker, D.E. Blahnik, CCTL Mark I and Mark II Prototype FFTF Subassembly Compression Test Development Work, WHAN-FR-18, August 1970.

3. J.R. Punches, S. Kaplan, Core Design Internal Document CD-001, "Advanced Wire-Wrap Assemblies Design Configurations and Rationale", GE-SAN 893-11-425, January 1974.

4. Nuclear Systems Materials Handbook, Volume I, TID 26666, Hanford Engineering Development Laboratory, Richland, Washington.

APPENDIX

WIRELESS ROD IRRADIATION IN EBR-II WIRE-WRAPPED BUNDLES

In discussing "wireless" bundles, it should be noted that such a fuel assembly design is currently being irradiated in EBR-II. The test vehicle is a reconstituted high-cladding-temperature experiment including irradiated fuel rods from the subassembly X141. These rods had reached approximately 5 atom % burnup with a maximum cladding temperature of 1300°F (704°C) at the time X141 was removed from the reactor. F11A, the reconstituted test, includes 34 of the X141 rods (with a 6-inch wire pitch) in a new MKJ 37 subassembly and three spare F9E wireless fuel rods. The wireless rods are installed two rows from the central rod, one row in from the hexagonal channel, and spaced between the wrapped rods, thereby providing adequate support by the six adjacent rods.

At present F11A has been removed for inspection at approximately 6-7 atom % due to cladding failure of one rod. This failure occurred in a wire-wrapped fuel rod away from the wireless rods. Hence, rod failure is not attributed to the wireless rods. Continued irradiation is scheduled in the near future with plans to increase the number of wireless rods (up to a maximum of seven rods), thereby offering further irradiation experience with a bundle including wireless fuel rods.

An inspection of the wireless rods provided evidence of obscure, incipient rod wear.* However, the wear was no more severe than that for standard wire-wrapped rods. Rod fretting and wear is, in general, caused by interactions between the rod cladding with neighboring rod wire wrapping rather than by interactions between the fuel rod cladding and its associated wire wrap. Removal of wire wraps does offer the potential of less rod wear and fretting because of the fewer contact locations.

---

*Hilbert, R. (GE), and Keys, R. (ANL), "Hot Fuel Examination Report (HFEF)," EBR-II Unpublished inspection report, January 14-15, 1976.

F11A provides encouraging evidence of satisfactory bundle performance during irradiation with some wireless rods. The total burnup of these wireless rods to date is low. Additional irradiation time is needed to assess fully the performance of wireless rods in EBR-II wire-wrapped bundles.